

PLASMONIC INTERACTION BETWEEN NANOSPHERES

SANGHYEON YU* AND HABIB AMMARI*

Abstract. When metallic (or plasmonic) nanospheres are nearly touching, strong concentration of light can occur in the narrow gap regions. This phenomenon has a potential application in nanophotonics, biosensing and spectroscopy. The understanding of the strong interaction between the plasmonic spheres turns out to be quite challenging. Indeed, an extremely high computational cost is required to compute the electromagnetic field. Also, the classical method of image charges, which is effective for dielectric spheres system, is not valid for plasmonic spheres because of their negative permittivities. Here we develop new analytical and numerical methods for the plasmonic spheres system by clarifying the connection between transformation optics and the method of image charges. We derive fully analytic solutions valid for two plasmonic spheres. We then develop a hybrid numerical scheme for computing the field distribution produced by an arbitrary number of spheres. Our method is highly efficient and accurate even in the nearly touching case and is valid for plasmonic spheres.

Key words. plasmon resonance, metallic nanospheres, transformation optics, method of image charges, analytic solution, hybrid numerical scheme

AMS subject classifications. 35J05, 65N80, 78A25

1. Introduction. Controlling light at the nanoscale is a challenging problem. By using conventional optical devices, one cannot focus light into a spot smaller than a micron-sized region due to the diffraction limit. To overcome this fundamental difficulty, new optical materials are required. Recently, noble metal nanoparticles such as gold and silver have been extensively studied and utilized due to their unique optical properties. When visible light is incident, the electromagnetic fields near the surfaces of the particles show strongly resonant and oscillating behavior. In other words, they can strongly interact with light. This phenomenon is called the plasmon resonance. So metallic nanoparticles are often called plasmonic nanoparticles. For practical applications of the plasmon resonance in nanophotonics, we refer to [18, 44, 48, 39, 37]. Roughly speaking, the plasmon resonance originates from the negative permittivity of metals. Contrary to plasmonic nanoparticles, ordinary dielectric nanoparticles with positive permittivity cannot strongly interact with light.

Among various plasmonic structures, the system of metallic spheres is of fundamental importance. When the spheres get close to touching, their interaction is so strong that plasmonic resonant fields can be greatly squeezed into the narrow gap region between them [38, 45, 50, 49, 35, 46]. Moreover, they can support collective resonance modes such as Fano resonances [30, 23]. These phenomena can have great impact on the design of nanophotonic devices, biosensing and spectroscopy [39, 37, 48, 18]. However, the problem of strong plasmonic interaction between nearly touching spheres is quite challenging to investigate both analytically and numerically.

We first discuss the analytic difficulty. There are two approaches for understanding the interaction between two spheres: (i) Transformation Optics (TO) and (ii) the method of image charges. TO is a design method for novel optical devices which control electromagnetic waves in an unprecedented way, including invisibility cloaks [40, 20, 13]. Recently, the TO approach has been applied to analyze various singular plasmonic structures. It provides a novel physical insight into light harvesting [39, 37]. In particular, TO gives exact analytical solutions for 2D systems. But, the 3D case

*Department of Mathematics, ETH Zürich, Rämistrasse 101, CH-8092 Zürich, Switzerland (sanghyeon.yu@sam.math.ethz.ch, habib.ammari@math.ethz.ch).

is more complicated. For two 3D plasmonic spheres, Pendry et al. [38] derived a quasi-analytic solution using a TO inversion mapping which transforms two spheres into a concentric shell. But their solution is not fully analytic and still requires a numerical computation.

Next we consider the method of image charges. The principle of the image method is to find fictitious sources which generate the desired field. For two 2D dielectric cylinders, an exact image series solution and its asymptotic properties were derived [33, 32, 3]. See also [1, 7, 8, 9, 16, 26, 51]. Although the 3D case is more difficult, Poladian succeeded in deriving an approximate but fully analytical image series solution for two 3D dielectric spheres [43, 41, 42]. Unfortunately, the image series solution is not convergent when the permittivity is negative. So it cannot describe the plasmonic interaction between two spheres. Therefore, both TO and the image method cannot provide a complete analytical description valid for two plasmonic spheres.

We now discuss the numerical difficulty. Let us consider an arbitrary number of spheres. If the spheres are well separated, computing the field distribution can be efficiently done. However, as the spheres get closer, the required computational cost dramatically increases. In this case, the field in the narrow gap between the spheres becomes nearly singular. So the multipole expansion method requires a large number of spherical harmonics and the finite element method (or boundary element method) requires a very fine mesh in the gap. Moreover, the linear systems to be solved are ill-conditioned. So conventional numerical methods are time consuming or inaccurate for this extreme case. Although TO approach provides an efficient numerical scheme, it cannot be applied when the number of spheres is greater than two. For an arbitrary number of 2D dielectric cylinders, Cheng and Greengard developed a hybrid numerical scheme combining the multipole expansion and the method of image charges [12]. They used the image source series to capture the close-to-touching interaction. Their scheme is extremely efficient and accurate even if the spheres are nearly touching. Their scheme has been generalized to 3D perfect conducting spheres [10] and 3D dielectric spheres [15]. However, as already mentioned, the image series is not convergent when the permittivity of the sphere is negative. Hence their hybrid scheme cannot be used for plasmonic sphere clusters. In short, there are currently no efficient numerical schemes for nearly touching plasmonic spheres system.

The purpose of this paper is to solve all these analytical and numerical difficulties. Specifically, our goal is twofold: (i) to derive a fully analytical solution for two plasmonic spheres, (ii) to develop a hybrid numerical scheme for computing the field generated by an arbitrary number of plasmonic spheres which are nearly touching.

The key idea of our approach is to establish a connection between TO and the method of image charges, which is interesting in itself. Indeed, we find explicit formulas which can convert image source series into TO-type solutions. As already mentioned, the image series cannot describe the plasmonic interaction due to the non-convergence. So we convert Poladian's image series solution into a TO-type series by using our connection formula, resulting in fully analytical solutions valid for two plasmonic spheres. Next we modify Cheng and Greengard's hybrid numerical scheme by replacing the image series with our new analytic TO-type solutions. We also show extreme efficiency and accuracy of the resulting scheme by presenting several numerical examples. Our proposed scheme is a result of the interplay between three analytical approaches: TO, the image method, and the multipole expansion. We expect that our results will play a fundamental role in studying the plasmonic interaction between nanospheres.

2. Problem formulation. We consider a system of N spheres $B_j, j = 1, 2, \dots, N$ where each individual sphere B_j has permittivity ϵ_B and radius R . We assume that the background has the permittivity $\epsilon_0 = 1$. Since the plasmonic nanospheres are much smaller than the wavelength of the visible light, we can adopt the quasi-static approximation for the electromagnetic fields. Then the electric field \mathbf{E} is represented as $\mathbf{E}(\mathbf{r}, t) = \Re\{-\nabla V(\mathbf{r})e^{i\omega t}\}$ where V is the (quasi-static) electric potential and ω is the frequency. We also assume a uniform incident field with intensity E_0 is applied in the z -direction. Then the potential V satisfies

$$(1) \quad \begin{cases} \nabla \cdot (\epsilon \nabla V) = 0, & \text{in } \mathbb{R}^3, \\ V(\mathbf{r}) = -E_0 z + O(|\mathbf{r}|^{-2}), & \text{as } |\mathbf{r}| \rightarrow \infty, \end{cases}$$

where ϵ is the permittivity distribution which takes the value ϵ_B (or $\epsilon_0 = 1$) on each sphere (or on the background), respectively. It can be shown that the above equation is equivalent to the following transmission problem:

$$(2) \quad \begin{cases} \Delta V = 0, & \text{in } \mathbb{R}^3 \setminus (\cup_{j=1}^N \partial B_j), \\ V|_- = V|_+, & \text{on } \partial B_j, \quad j = 1, 2, \dots, N, \\ \epsilon_B \frac{\partial V}{\partial \mathbf{n}}|_- = \frac{\partial V}{\partial \mathbf{n}}|_+, & \text{on } \partial B_j, \quad j = 1, 2, \dots, N, \\ V(\mathbf{r}) = -E_0 z + O(|\mathbf{r}|^{-2}), & \text{as } |\mathbf{r}| \rightarrow \infty, \end{cases}$$

where \mathbf{n} is an outward unit normal vector and the subscript $+$ (or $-$) means the limit from outside (or inside), respectively.

The permittivity ϵ_B of each metallic sphere depends on the frequency ω . According to the Drude model, ϵ_B is modeled as

$$(3) \quad \epsilon_B = \epsilon_B(\omega) = 1 - \frac{\omega_p^2}{\omega(\omega + i\gamma)},$$

where $\omega_p > 0$ is the plasma frequency and $\gamma > 0$ is a small damping parameter. It is clear that $\Re\{\epsilon_B\} < 0$ for $\omega < \omega_p$. Note that, as $\omega \rightarrow 0$, the permittivity $|\epsilon_B|$ goes to infinity. In this paper, we assume a silver nanoparticle and fit Palik's data [36] for silver by adding a few Lorentz terms to (3). For specific values of the fitting parameters, see [53].

3. Plasmon resonance. Here we briefly discuss the mathematical structure of plasmonic resonant fields. Recently, a rigorous and general theory of plasmon resonances for nanoparticles has been developed using the spectral analysis of the Neumann-Poincaré (NP) operator in [2, 6, 4, 5]. We emphasize that the theory is valid for arbitrary shaped particles with smooth boundary. There, it was shown that there is a sequence $\{\epsilon_n\}_{n=1}^{\infty}$ of negative real permittivities such that $\epsilon_1 \leq \epsilon_2 \leq \dots < -1$ and there exists a nontrivial solution V_n to the problem (2) with $\epsilon_B = \epsilon_n$ and $E_0 = 0$. Moreover, the solution V to the original problem (2) can be written in the following spectral form (it is slightly modified for our purpose):

$$(4) \quad V(\mathbf{r}) = -E_0 z + \sum_{n=1}^{\infty} \frac{c_n}{\epsilon_B - \epsilon_n} V_n(\mathbf{r}),$$

where the c_n are some constant coefficients. Typically, the solution V_n shows oscillating behavior along the boundary of the particles. These solutions V_n are called the

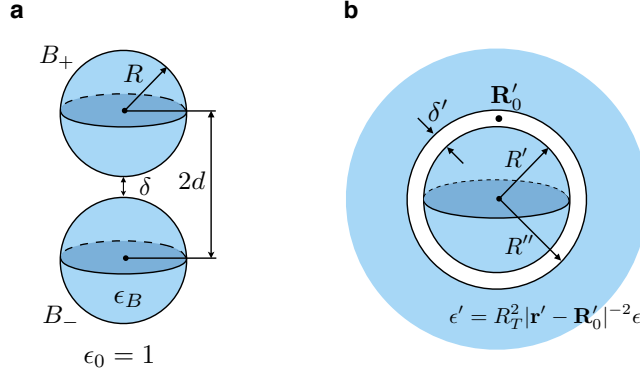


FIG. 1. *Two spheres and the TO inversion mapping. (a) Two identical spheres, each of radius R and the permittivity ϵ_B , are separated by a distance δ . The distance between their centers is $2d$. The background permittivity is $\epsilon_0 = 1$. (b) The TO inversion mapping transforms the lower sphere B_- (or the upper sphere B_+) into a sphere of radius R' (or a hollow sphere of radius R'') centered at the origin, respectively.*

plasmon resonance modes. We also call ϵ_n as the plasmonic resonant permittivities. It is also worth mentioning that $\lambda_n := (\epsilon_n + 1)/(2(\epsilon_n - 1))$ are eigenvalues of the NP operator and V_n is a single layer potential of the eigenfunction associated to λ_n .

The formula (4) clearly shows how the plasmon resonance occurs. As already mentioned, the real part of $\epsilon_B(\omega)$ can take any negative values from 0 to $-\infty$ for $\omega < \omega_p$. So ϵ_B can be close to some resonant permittivity ϵ_n since $\epsilon_n < -1$. Then, in view of (4), we see that the associated plasmon resonance mode V_n will be amplified. As a result, the nanoparticles strongly couple with the incident light. On the contrary, if the permittivity ϵ_B is positive, the plasmon resonance never occurs.

4. Transformation Optics approach for two spheres. Here we briefly review the TO approach by Pendry et al. [38]. Let us assume there are only two spheres, *i.e.*, $N = 2$. We first need to fix notations. Suppose that two spheres B_1 and B_2 are centered at $(0, 0, +d)$ and $(0, 0, -d)$, respectively. For convenience, let us denote $B_1 = B_+$ and $B_2 = B_-$. We also let δ be the gap distance between the two spheres. See Figure 1a.

To transform two spheres into a concentric shell, Pendry et al. [38] introduced the inversion transformation Φ defined as

$$\mathbf{r}' = \Phi(\mathbf{r}) = R_T^2(\mathbf{r} - \mathbf{R}_0)/|\mathbf{r} - \mathbf{R}_0|^2 + \mathbf{R}'_0,$$

where $\mathbf{R}_0, \mathbf{R}'_0$ and R_T are given parameters (for the details, see Appendix B). Then the transformed potential $V' := V \circ \Phi^{-1}$ satisfies $\nabla \cdot (\epsilon' \nabla V') = 0$ where ϵ' is the transformed permittivity distribution defined by $\epsilon'(\mathbf{r}') = R_T^2 |\mathbf{r}' - \mathbf{R}'_0|^{-2} \epsilon$. Then, by taking advantage of the symmetry of the shell, they represented the potential V in terms of the following basis functions:

$$\mathcal{M}_{n,\pm}^m(\mathbf{r}) = |\mathbf{r}' - \mathbf{R}'_0| (r')^{\pm(n+\frac{1}{2})-\frac{1}{2}} Y_n^m(\theta', \phi'),$$

where Y_n^m are the spherical harmonics. We will call $\mathcal{M}_{n,\pm}^m$ a TO basis.

Then the potential V outside the two spheres in a uniform field $(0, 0, E_0)$ can be

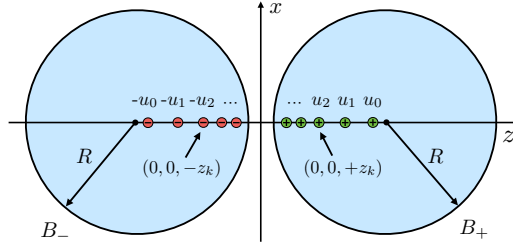


FIG. 2. *Image charges for two spheres. Red and green circles represent image charges placed along the z-axis.*

represented as follows:

$$(5) \quad V(\mathbf{r}) = -E_0 z + \sum_{n=0}^{\infty} A_n (\mathcal{M}_{n,+}^0(\mathbf{r}) - \mathcal{M}_{n,-}^0(\mathbf{r})).$$

Here, the coefficients A_n can be determined by solving some tridiagonal system or recurrence relations (see Appendix C for the details). Unfortunately, it cannot be solved analytically and a numerical computation is required to get the A_n . It is worth mentioning that Goyette and Navon [17] derived a similar solution using bispherical coordinates.

We will derive an approximate analytical expression for A_n by establishing the explicit connection between TO and the method of image charges. We shall also see that our approximate expression captures the singular nature of the close-to-touching interaction completely.

5. Method of image charges for two spheres. Now we discuss the method of images. In the case of two 2D circular cylinders, the exact solution is represented as an infinite series of image point sources. McPhedran, Poladian and Milton [33] derived its asymptotic properties in the nearly touching case by approximating the sequence of image charges or dipoles. However, for two 3D dielectric spheres, an exact solution cannot be obtained due to the appearance of a continuous line image source [28, 29, 34]. Poladian observed that the continuous source can be well approximated by a point charge and then the imaging rule becomes similar to the 2D case. He then derived an approximate but analytic image series solution and its asymptotic properties [43, 41, 42]. See also [7, 16, 21, 22, 24, 25, 27, 52].

Let us briefly state Poladian's solution for two 3D dielectric spheres (for the reader's convenience, we include the details of Poladian's image method in Appendix D). Let $\tau = (\epsilon_B - 1)/(\epsilon_B + 1)$, $s = \cosh^{-1}(d/R)$ and $\alpha = R \sinh s$. Suppose that two point charges of strength ± 1 are located at $(0, 0, \pm z_0) \in B_{\pm}$, respectively. By Poladian's imaging rule, they produce an infinite series of image charges of strength $\pm u_k$ at $(0, 0, \pm z_k)$ for $k = 0, 1, 2, \dots$, where z_k and u_k are given by

$$(6) \quad z_k = \alpha \coth(ks + s + t_0), \quad u_k = \tau^k \frac{\sinh(s + t_0)}{\sinh(ks + s + t_0)}.$$

Here, the parameter t_0 is such that $z_0 = \alpha \coth(s + t_0)$. See Figure 2. The potential

$U(\mathbf{r})$ generated by all the above image charges is given by

$$(7) \quad U(\mathbf{r}) = \sum_{k=0}^{\infty} u_k (G(\mathbf{r} - \mathbf{z}_k) - G(\mathbf{r} + \mathbf{z}_k)),$$

where $\mathbf{z}_k = (0, 0, z_k)$ and $G(\mathbf{r}) = 1/(4\pi|\mathbf{r}|)$ is the potential generated by a unit point charge located at the origin.

Let us turn to the solution V to the problem (2), which is the potential generated by the two spheres $B_+ \cup B_-$ under a uniform incident field $(0, 0, E_0)$. Let p_0 be the induced polarizability when a single sphere is subjected to the uniform incident field, that is, $p_0 = E_0 R^3 2\tau/(3 - \tau)$. Using the potential $U(\mathbf{r})$, we can represent the approximate solution for $V(\mathbf{r})$ as follows (see Appendix D.2 for its derivation): for $|\tau| \approx 1$, we have

$$(8) \quad V(\mathbf{r}) \approx -E_0 z + 4\pi p_0 \frac{\partial(U(\mathbf{r}))}{\partial z_0} \Big|_{z_0=d} + QU(\mathbf{r})|_{z_0=d},$$

where Q is a constant chosen so that the right-hand side in equation (8) has no net flux on the surface of each sphere. The accuracy of the approximate formula (8) improves as $|\epsilon_B|$ increases and it becomes exact when $|\epsilon_B| = \infty$. Moreover, its accuracy is pretty good even if the value of $|\epsilon_B|$ is moderate.

We now explain the difficulty in applying the the image series solution (8) to the plasmonic spheres. In view of the expressions (6) for u_k , we can see that the image series solution (8) is not convergent when $|\tau| > e^s$. For plasmonic materials such as gold and silver, the real part of the permittivity ϵ_B is negative over optical frequencies and then the corresponding parameter $|\tau|$ can attain any value in the interval (e^s, ∞) . Moreover, it turns out that all the plasmonic resonant values for τ are contained in the set $\{\tau \in \mathbb{C} : |\tau| > e^s\}$. So, the image method solution (8) cannot describe the plasmonic interaction between the spheres due to the non-convergence.

6. Connection formula from image charges to TO. Now we clarify the connection between TO and the method of image charges. We derive an explicit formula which converts an image charge to TO-type solutions as shown in the following lemma (see Appendix E for its proof).

LEMMA 6.1. (*Converting an image charge to TO*) *The potential $u_k G(\mathbf{r} \mp \mathbf{z}_k)$ generated by the image charge at $\pm \mathbf{z}_k$ can be rewritten using the TO basis as follows: for $\mathbf{r} \in \mathbb{R}^3 \setminus (B_+ \cup B_-)$,*

$$(9) \quad u_k G(\mathbf{r} \mp \mathbf{z}_k) = \frac{\sinh(s + t_0)}{4\pi\alpha} \sum_{n=0}^{\infty} [\tau e^{-(2n+1)s}]^k e^{-(2n+1)(s+t_0)} \mathcal{M}_{n,\pm}^0(\mathbf{r}).$$

This identity plays a key role in our derivation of the approximate analytical solution. As mentioned previously, the reason why the image charge series (7) does not work for plasmonic spheres is because the factor $(\tau e^{-s})^k$ may not converge to zero as $k \rightarrow \infty$. But the above connection formula helps us overcome this difficulty. If we sum up all the image charges in equation (9), we can see that the summation over k can be evaluated analytically using the following identity:

$$\sum_{k=0}^{\infty} [\tau e^{-(2n+1)s}]^k = \frac{e^{(2n+1)s}}{e^{(2n+1)s} - \tau}.$$

Therefore, from (7) and Lemma 6.1, we obtain the following result.

THEOREM 6.2. *(Converting image charge series to TO) Let $U(\mathbf{r})$ be the image charge series defined as in (7). Then it can be rewritten using TO basis as follows: for $\mathbf{r} \in \mathbb{R}^3 \setminus (B_+ \cup B_-)$,*

$$(10) \quad U(\mathbf{r}) = \frac{\sinh(s+t_0)}{4\pi\alpha} \sum_{n=0}^{\infty} \frac{e^{-(2n+1)t_0}}{e^{(2n+1)s} - \tau} \left(\mathcal{M}_{n,+}^0(\mathbf{r}) - \mathcal{M}_{n,-}^0(\mathbf{r}) \right).$$

Clearly, the right-hand side of (10) does converge for any $|\tau| > e^s$ provided that $\tau \neq e^{(2n+1)s}$.

7. Analytical solution for two plasmonic spheres. Here we derive an analytical approximate solution V for two plasmonic spheres in a uniform incident field $(0, 0, E_0)$. Moreover, we shall see that our analytical approximation completely captures the singular behavior of the exact solution. This feature will be essentially used to develop our hybrid numerical scheme. We only consider the case when the incident field is in the direction of the z -axis. In the case of the x or y -axis, a high field concentration in the gap does not happen [38, 45].

To derive the solution valid for two plasmonic spheres, we convert the image series (8) into a TO-type solution by using the connection formula (10). The result is shown in the following theorem (see Appendix F for its proof).

THEOREM 7.1. *If $|\tau| \approx 1$, the following approximation for the electric potential $V(\mathbf{r})$ holds: for $\mathbf{r} \in \mathbb{R}^3 \setminus (B_+ \cup B_-)$,*

$$(11) \quad V(\mathbf{r}) \approx -E_0 z + \sum_{n=0}^{\infty} \tilde{A}_n \left(\mathcal{M}_{n,+}^0(\mathbf{r}) - \mathcal{M}_{n,-}^0(\mathbf{r}) \right),$$

where the coefficient \tilde{A}_n is given by

$$\begin{aligned} \tilde{A}_n &= E_0 \frac{2\tau\alpha}{3-\tau} \cdot \frac{2n+1-K_0}{e^{(2n+1)s} - \tau}, \\ K_0 &= \sum_{n=0}^{\infty} \frac{2n+1}{e^{(2n+1)s} - \tau} \bigg/ \sum_{n=0}^{\infty} \frac{1}{e^{(2n+1)s} - \tau}. \end{aligned}$$

As expected, the above approximate expression is valid even if $|\tau| > e^s$. Therefore, it can furnish useful information about the plasmonic interaction between the two spheres. As a first demonstration, let us investigate the (approximate) resonance condition, that is, the condition for τ at which the coefficients \tilde{A}_n diverge. One might conclude that the resonance condition is given by $\tau = e^{(2n+1)s}$. However, one can see that \tilde{A}_n has a removable singularity at each $\tau = e^{(2n+1)s}$. In fact, the (approximate) resonance condition turns out to be

$$(12) \quad \sum_{n=0}^{\infty} \frac{1}{e^{(2n+1)s} - \tau} = 0.$$

In other words, the plasmon resonance does happen when τ is one of zeros of equation (12). It turns out that the zeros $\{\tau_n\}_{n=0}^{\infty}$ lie on the positive real axis and satisfy, for $n = 0, 1, 2, \dots$,

$$(13) \quad e^{(2n+1)s} < \tau_n < e^{(2n+3)s}.$$

The above estimate help us understand the asymptotic behavior of the resonance when two spheres get closer. As the gap distance δ goes to zero, the parameter s

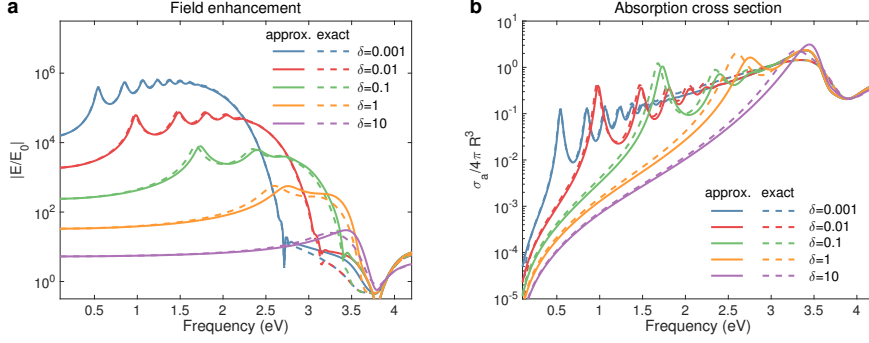


FIG. 3. *Exact solution vs Analytic approximation.* (a) Field enhancement plot as a function of the frequency ω for various separation distances δ . The solid lines represent the approximate analytical solution and the dashed lines represent the exact solution. Two identical silver spheres of radius 30 nm are considered. (b) Same as (a) but for the absorption cross section.

also goes to zero (in fact, $s = O(\delta^{1/2})$). Then, in view of (13), τ_n will converge to 1 and the corresponding permittivity $|\epsilon_n|$ goes to infinity. Also, the corresponding frequency ω_n goes to zero according to Drude's model. This phenomenon is sometimes called the red-shift of the (bright) resonance modes [45, 46]. Since our approximate analytical formula (11) for V becomes more accurate as $|\epsilon_B|$ increases, we can expect that accuracy of the plasmonic resonant field improves as the separation distance goes to zero. It also indicates that our formula captures the singular nature of the field distribution completely. Also, the difference between τ_n and τ_{n+1} decreases, which means that the spectrum becomes a nearly continuous one. It is worth mentioning that $1/(2\tau_n)$ gives the approximate eigenvalues of the Neumann-Poincaré operator for two spheres.

We now derive approximate formulas for the field at the gap center and for the absorption cross section. From Theorem 7.1, we obtain the following approximation (see Appendix H for the details):

$$E(0, 0, 0) \approx E_0 - E_0 \frac{8\tau}{3 - \tau} \left[\sum_{n=0}^{\infty} \frac{(2n+1)^2}{e^{(2n+1)s} - \tau} (-1)^n - K_0 \sum_{n=0}^{\infty} \frac{2n+1}{e^{(2n+1)s} - \tau} (-1)^n \right].$$

In the quasi-static approximation, the absorption cross section σ_a is defined by $\sigma_a = \omega \text{Im}\{p\}$, where p is the polarizability of the system of two spheres. From Theorem 7.1, σ_a is approximated as follows (see again Appendix H):

$$\sigma_a \approx \omega E_0 \frac{8\tau\alpha^3}{3 - \tau} \left[\sum_{n=0}^{\infty} \frac{(2n+1)^2}{e^{(2n+1)s} - \tau} - \left(\sum_{n=0}^{\infty} \frac{2n+1}{e^{(2n+1)s} - \tau} \right)^2 / \sum_{n=0}^{\infty} \frac{1}{e^{(2n+1)s} - \tau} \right].$$

We compare the above approximate formulas with the exact ones. Figure 3 represents respectively the field enhancement and the absorption cross section σ_a as functions of the frequency ω for various distances ranging from 0.001 nm to 10 nm.

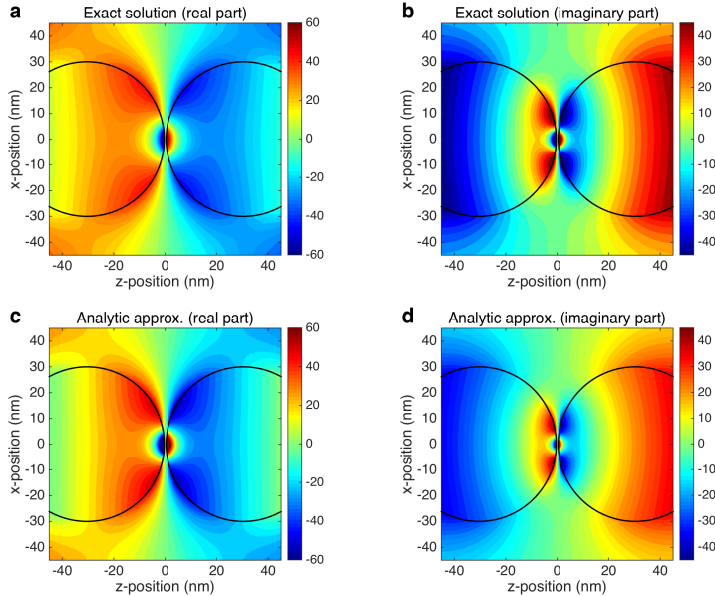


FIG. 4. Potential distributions for two identical silver spheres of radius 30 nm separated by $\delta = 0.25$ nm. (a,b) Real and imaginary parts of the exact solution. The uniform incident field $(0, 0, \text{Re}\{e^{i\omega t}\})$ is applied at the frequency $\omega = 3.0$ eV in z -direction. (c,d) Same as (a,b) but for the analytical approximate solution.

The good accuracy of our approximate formulas over broad ranges of frequencies and gap distances is clearly shown. As mentioned previously, the accuracy improves as the spheres get closer. The red-shift of the plasmon resonance modes is also shown. It is worth to mention that Schnitzer [46] performed an asymptotic analysis for the field enhancement, the polarizability and their red-shift behavior. In Figure 4, we compare the exact and approximate electric potential distributions. They are also in good agreement and the field concentration in the gap region is observed.

8. Hybrid numerical scheme for many-spheres system. Now we consider a system of an arbitrary number of plasmonic spheres. If all the spheres are well separated, then the multipole expansion method is efficient and accurate for computing the field distribution (see Appendix I). But, when the spheres are close to each other, the problem becomes very challenging since the charge densities on each sphere are nearly singular. To overcome this difficulty, Cheng and Greengard developed a hybrid numerical scheme combining the multipole expansion and the method of images [12]. See also [10, 15].

Let us briefly explain the main idea of Cheng and Greengard's method. In the standard multipole expansion method, the potential is represented as a sum of general multipole sources $\mathcal{Y}_{lm}(\mathbf{r}) = Y_l^m(\theta, \phi)/r^{l+1}$ located at the center of each of spheres. Suppose that a pair of spheres is close to touching. For convenience, let us identify the pair as $B_+ \cup B_-$. A multipole source \mathcal{Y}_{lm} located at the center of B_+ generates an infinite sequence of image multipole sources by Poladian's imaging rule. Let us denote the resulting image multipole potential by U_{lm}^+ . We also define U_{lm}^- in a similar way. The detailed image series representation for U_{lm}^\pm can be found in Appendix D.3. Roughly speaking, Cheng and Greengard modified the multipole expansion by replacing a multipole source \mathcal{Y}_{lm} with its corresponding image multipole series U_{lm}^\pm .

Since the image series U_{lm}^\pm captures the close-to-touching interactions analytically, their scheme is extremely efficient and highly accurate even if the distance between the spheres is extremely small. However, the image multipole series U_{lm}^\pm are not convergent for $|\tau| > e^s$. Hence it cannot be applied to plasmonic spheres clusters. Therefore, for extending Cheng and Greengard's method to the plasmonic case, it is essential to establish an explicit connection between the image multipole series U_{lm}^\pm and TO. We derive the following formula for this connection (see Appendix G for its proof).

THEOREM 8.1. *(Converting image multipole series to TO) Assume that the integers l and m are such that $l \geq 1$ and $-l \leq m \leq l$. The potential U_{lm}^\pm can be rewritten in terms of TO basis as follows: for $\mathbf{r} \in \mathbb{R}^3 \setminus (B_+ \cup B_-)$,*

$$(14) \quad \begin{aligned} U_{lm}^\pm(\mathbf{r}) &= \sum_{n=|m|}^{\infty} \frac{g_n^m \mathcal{D}_{lm}^\pm[\lambda_n^m]}{e^{2(2n+1)s} - \tau^2} (e^{(2n+1)s} \mathcal{M}_{n,\pm}^m(\mathbf{r}) - \tau \mathcal{M}_{n,\mp}^m(\mathbf{r})) \\ &\quad - \delta_{0m} \frac{\tilde{Q}_{l,1}^\pm}{2} \sum_{n=0}^{\infty} \frac{\mathcal{M}_{n,+}^0(\mathbf{r}) + (-1)^l \mathcal{M}_{n,-}^0(\mathbf{r})}{e^{(2n+1)s} + (-1)^l \tau} \\ &\quad \mp \delta_{0m} \frac{\tilde{Q}_{l,2}^\pm}{2} \sum_{n=0}^{\infty} \frac{\mathcal{M}_{n,+}^0(\mathbf{r}) - (-1)^l \mathcal{M}_{n,-}^0(\mathbf{r})}{e^{(2n+1)s} - (-1)^l \tau}, \end{aligned}$$

where g_n^m , λ_n^m and Q_l^\pm are given by

$$(15) \quad \begin{aligned} g_n^m &= \frac{1}{\alpha^{|m|+1}} \frac{2^{|m|}}{\sqrt{(2|m|)!}} \sqrt{\frac{(n+|m|)!}{(n-|m|)!}}, \\ \lambda_n^m &= [\sinh(s+t_0)]^{2|m|+1} e^{-(2n+1)t_0}, \\ \tilde{Q}_{l,i}^\pm &= \sum_{n=0}^{\infty} \frac{(\pm 1)^l g_n^0 \mathcal{D}_{l0}^\pm[\lambda_n^0]}{e^{(2n+1)s} - (-1)^{l+i} \tau} \bigg/ \sum_{n=0}^{\infty} \frac{1}{e^{(2n+1)s} - (-1)^{l+i} \tau}. \end{aligned}$$

Here, $\mathcal{D}_{lm}^\pm[\cdot]$ is defined by (34) and δ_{lm} is the Kronecker's delta function.

Clearly, the above TO representation for U_{lm}^\pm does converge for $|\tau| > e^s$. Based on these analytic formulas, we develop a modified hybrid numerical scheme for the plasmonic spheres system. Specifically, we modify Cheng and Greengard's hybrid scheme by replacing the image multipole series U_{lm}^\pm with its TO version using Theorem 8.1. The resulting hybrid scheme is valid for plasmonic spheres. Our new analytic TO-type solutions for U_{lm}^\pm capture the singular behavior of the field distribution in the gap regions. So our modified hybrid scheme is extremely efficient and accurate even when the spheres are nearly touching. For a detailed description of the proposed scheme, we refer to Appendix J.

Next, we present numerical examples to illustrate the hybrid method. We consider two examples of the three-spheres configuration shown in Figures 5a and 5d. We show comparison between multipole expansion method and the hybrid method by plotting the field enhancement at the gap center A . For the numerical implementation, only a finite number of the multipoles \mathcal{Y}_{lm} or hybrid multipoles U_{lm}^\pm should be used. Let L be the truncation number for the order l . In Figures 5b and 5e, the field enhancement is computed using the standard multipole expansion method. The computations give inaccurate results even if we include a large number of multipole sources with $L = 50$. On the contrary, the hybrid method gives pretty accurate results even for small values of L such as $L = 2$ and 5; see Figures 5c and 5f. Also, 99% accuracy can be achieved

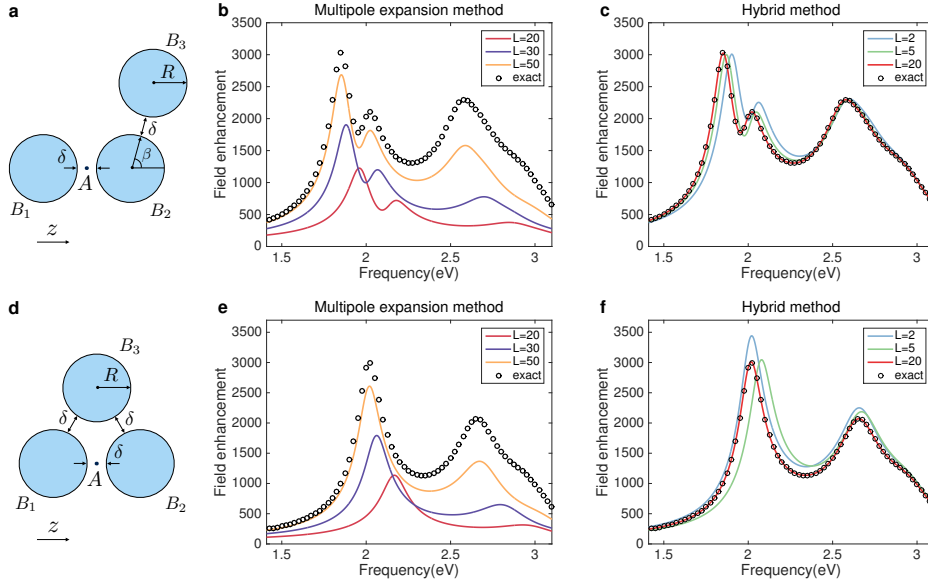


FIG. 5. *Multipole expansion method vs Hybrid scheme.* (a,d) Two examples of three spheres configurations. (b,c) The field enhancement at point A as a function of frequency for the configuration (a) using the multipole expansion method and the hybrid method, respectively. The parameters are given as $R = 30$ nm, $\delta = 0.25$ nm and $\beta = 80^\circ$. The uniform incident field $(0, 0, \text{Re}\{e^{i\omega t}\})$ is applied (e,f) Same as (b,c) but for the configuration (d).

only with $L = 20$. For each hybrid multipole U_{lm}^\pm , the TO harmonics are included up to order $n = 300$ to ensure convergence and it can be evaluated very efficiently.

To achieve 99.9% accuracy at the first resonant peak, it is required to set $L = 150$ in the multipole expansion method and a $68,400 \times 68,400$ linear system needs to be solved. However, the same accuracy can be achieved only with $L = 23$ in the hybrid method. The corresponding linear system's size is $1,725 \times 1,725$ and it can be solved 2,000 times faster than that of the multipole expansion method. In Figure 6, we also show the field distribution for the three-spheres examples. The high field concentration in the narrow gap regions between nanospheres is clearly shown.

9. Discussion. In this paper, we have fully characterized the singular nature of interaction between nearly touching plasmonic nanospheres in an analytical way. Based on new analytic solutions, we also have extended Cheng and Greengard's hybrid numerical method to the case of plasmonic spheres. The extended scheme gives extreme efficiency and accuracy for computing the field generated by an arbitrary number of plasmonic spheres even when they are nearly touching. We have assumed that the spheres are identical only for simplicity. Our approach can be directly extended to the case where the spheres are not equisized and have different material parameters. Moreover, by coupling with the fast multipole method, we expect that the proposed scheme will give an efficient numerical solver for a large scale problem [19, 11]. In that case, we should consider the retardation effect which comes from the finite wavelength of the incident light. But the quasistatic interaction is dominant for any pair of closely spaced spheres and so our result is still useful in a large scale problem. This will be the subject of a forthcoming paper. The nonlocal effect, which has a quantum mechanical origin, is an important issue when the spheres are extremely

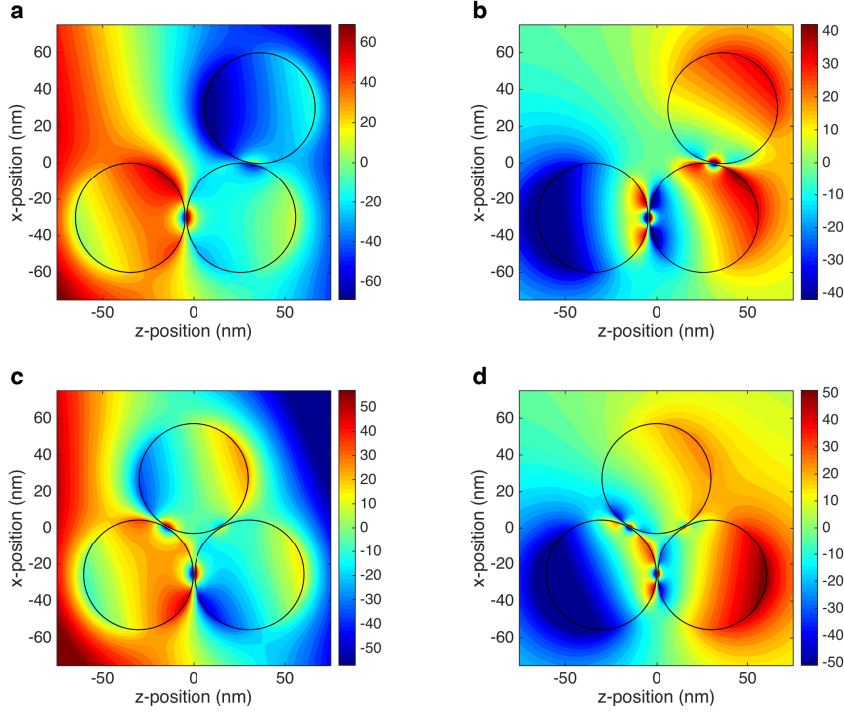


FIG. 6. Potential distributions for the two three spheres examples. (a,b) Real and imaginary parts of the potential for the configuration in Figure 5a with $R = 30$ nm, $\delta = 0.25$ nm, and $\beta = 80^\circ$. The uniform incident field $(\sin 15^\circ, 0, \cos 15^\circ) \text{Re}\{e^{i\omega t}\}$ is applied at $\omega = 3.0$ eV. (c,d) Same as (a,b) but for the configuration in Figure 5d.

closely spaced [31, 14, 47]. By adopting the shifting boundary method developed by Luo et al. [31], this effect can be easily incorporated.

Appendix A. Some definitions and properties.

- Let us define the spherical harmonics Y_l^m by

$$Y_l^m(\theta, \phi) = \sqrt{\frac{(l - |m|)!}{(l + |m|)!}} P_l^{|m|}(\cos \theta) e^{im\phi},$$

where $P_l^m(x)$ is the associated Legendre polynomial given by

$$P_l^m(x) = (-1)^m (1 - x^2)^{m/2} \frac{d^m}{dx^m} P_l(x).$$

Here, $P_l(x)$ is the Legendre polynomial of degree l .

- The Legendre polynomial $P_n(x)$ has the following generating function:

$$(16) \quad \frac{1}{\sqrt{1 - 2ax + a^2}} = \sum_{n=0}^{\infty} a^n P_n(x).$$

- The associated Legendre polynomial $P_n^m(x)$ has the following generating function:

$$(17) \quad (-1)^m (2m - 1)!! \frac{(1 - x^2)^{m/2} a^m}{[1 - 2ax + a^2]^{m+1/2}} = \sum_{n=m}^{\infty} a^n P_n^m(x).$$

- It holds that

$$(18) \quad P_n^n(x) = (-1)^n (2n-1)!! (1-x^2)^{n/2}.$$

- Let us define the solid harmonics \mathcal{Y}_{lm} and \mathcal{Z}_{lm} by

$$\begin{aligned} \mathcal{Y}_{lm}(\mathbf{r}) &= r^{-(l+1)} Y_l^m(\theta, \phi), \\ \mathcal{Z}_{lm}(\mathbf{r}) &= r^l Y_l^m(\theta, \phi). \end{aligned}$$

The function \mathcal{Y}_{lm} is also called the multipole source.

- Let us introduce

$$(19) \quad w_m = \begin{cases} 1, & m \geq 0, \\ (-1)^{|m|}, & m < 0. \end{cases}$$

- Let the constant N_{lmab} be given by

$$(20) \quad N_{lmab} = (-1)^{a+b} \sqrt{\binom{l+a-b+m}{l+m} \binom{l+a+b-m}{a+b}},$$

and let the constant N_{lm} be given by

$$(21) \quad N_{lm} = (l-|m|)! \sqrt{\binom{l+|m|}{l+m} \binom{l+|m|}{|m|+m}}.$$

Appendix B. TO inversion mapping and the bispherical coordinates.

Here we present the basic properties of the TO inversion mapping. The TO inversion mapping Φ can be rewritten using the bispherical coordinates (ξ, η, φ) defined by

$$(22) \quad e^{\xi - i\eta} = (z + i\rho + \alpha)/(z + i\rho - \alpha),$$

with $\rho = \sqrt{x^2 + y^2}$ and φ being the azimuthal angle.

By letting $\mathbf{r}' = e^\xi (\sin \eta \cos \varphi, \sin \eta \sin \varphi, \cos \eta)$, $\mathbf{R}'_0 = (0, 0, 1)$, $\mathbf{R}_0 = (0, 0, \alpha)$ and $R_T^2 = 2\alpha$, we can see that the bispherical transformation is identical to the inversion mapping in the TO approach. Although they are the same, it is worth mentioning that TO approach gives novel physical insights into the interaction between two plasmonic spheres. The reason why we rewrite Φ in terms of the bispherical coordinates is that many useful properties have been derived in this coordinate system. In Figure 7, the geometry of the bispherical coordinates is described.

The Cartesian coordinates can be written in terms of the bispherical ones as follows:

$$(23) \quad x = \frac{\alpha \sin \eta \cos \varphi}{\cosh \xi - \cos \eta}, \quad y = \frac{\alpha \sin \eta \sin \varphi}{\cosh \xi - \cos \eta}, \quad z = \frac{\alpha \sinh \xi}{\cosh \xi - \cos \eta}.$$

Note that the origin $(0, 0, 0)$ corresponds to $\xi = 0, \eta = \pi, \varphi = 0$. The point at infinity corresponds to $(\xi, \eta) \rightarrow (0, 0)$. On the other hand, it can be easily shown that the coordinate surfaces $\{\xi = c\}$ and $\{\eta = c\}$ for a nonzero c are respectively the zero level set of

$$(24) \quad f^\xi(x, y, z) = (z - \alpha \coth c)^2 + \rho^2 - (\alpha/\sinh c)^2,$$

$$(25) \quad f^\eta(x, y, z) = (\rho - \alpha \cot c)^2 + z^2 - (\alpha/\sin c)^2.$$

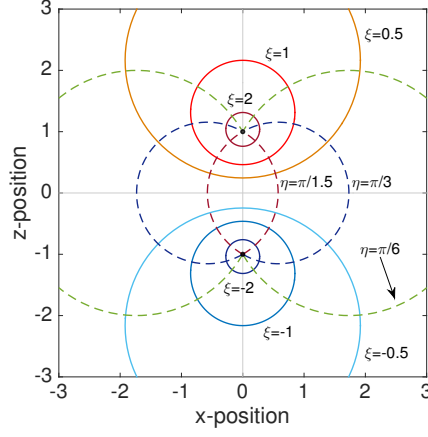


FIG. 7. *Bispherical coordinates.* Coordinate level curves for the bispherical coordinate system with $\alpha = 1$. The solid lines (resp. the dashed lines) represent ξ (resp. η) coordinate curves.

Note also that the ξ -coordinate surface is the sphere of radius $\alpha/\sinh c$ centered at $(0, 0, \alpha \coth c)$. Therefore, $\xi = c$ (or $\xi = -c$) represents a sphere contained in the region $z > 0$ (resp. $z < 0$). Moreover, $|\xi| < c$ (resp. $|\xi| > c$) represents the region outside (resp. inside) the two spheres.

Suppose that two spheres B_+ and B_- of the same radius R are centered at $(0, 0, +d)$ and $(0, 0, -d)$, respectively. We set $s = \cosh^{-1}(d/R)$ and $\alpha = R \sinh s$. Then we have $d = \alpha \coth s$ and $R = \alpha/\sinh s$. So, in view of (24), the surfaces $\{\partial B_{\pm}\}$ of the two spheres are parametrized by $\{\xi = \pm s\}$, respectively.

Any solution to the Laplace's equation can be represented as a sum of the following bispherical harmonics which is equal to the TO basis $\mathcal{M}_{n,\pm}^m$ as follows:

$$(26) \quad \mathcal{M}_{n,\pm}^m(\mathbf{r}) = \sqrt{2} \sqrt{\cosh \xi - \cos \eta} e^{\pm(n+\frac{1}{2})\xi} Y_n^m(\eta, \varphi).$$

The scale factors for the bispherical coordinates are

$$\sigma_{\xi} = \sigma_{\eta} = \frac{\alpha}{\cosh \xi - \cos \eta} \quad \text{and} \quad \sigma_{\varphi} = \frac{\alpha \sin \eta}{\cosh \xi - \cos \eta},$$

so that the gradient for a scalar valued function g can be written in the form

$$\nabla g = \frac{1}{\sigma_{\xi}} \frac{\partial g}{\partial \xi} \mathbf{e}_{\xi} + \frac{1}{\sigma_{\eta}} \frac{\partial g}{\partial \eta} \mathbf{e}_{\eta} + \frac{1}{\sigma_{\varphi}} \frac{\partial g}{\partial \varphi} \mathbf{e}_{\varphi},$$

where $\{\mathbf{e}_{\xi}, \mathbf{e}_{\eta}, \mathbf{e}_{\varphi}\}$ are the unit basis vectors in the bispherical coordinates. The normal derivative on the surface $\{\xi = \pm s\}$ of the sphere B_{\pm} is given by

$$(27) \quad \frac{\partial}{\partial \mathbf{n}} \Big|_{\partial B_{\pm}} = \mp \mathbf{e}_{\xi} \cdot \nabla \Big|_{\partial B_{\pm}} = \mp \frac{\cosh s - \cos \eta}{\alpha} \frac{\partial}{\partial \xi} \Big|_{\xi = \pm s},$$

where \mathbf{n} denotes the outward unit normal vector.

If the function g is of the following form:

$$g(\mathbf{r}) = \sum_{n=0}^{\infty} \sum_{m=-n}^n c_n^m \mathcal{M}_{n,+}^m(\mathbf{r}) + d_n^m \mathcal{M}_{n,-}^m(\mathbf{r}),$$

then z -component of the gradient at the origin is given by

$$(28) \quad \mathbf{e}_z \cdot \nabla g(0, 0, 0) = \frac{2^{3/2}}{\alpha} \sum_{n=0}^{\infty} (c_n^0 - d_n^0)(n + 1/2)(-1)^n,$$

where $\mathbf{e}_z = (0, 0, 1)$.

Appendix C. Recurrence relations for A_n . In [17], it was shown that the coefficients A_n in (5) satisfy the following recurrence relations: for $n = 0, 1, 2, \dots$,

$$(\bar{n} - 1/2)f_{n-1}A_{n-1} - g_nA_n + (\bar{n} + 1/2)f_{n+1}A_{n+1} = E_0h_n,$$

where $\bar{n} = n + 1/2$, $A_{-1} = 0$ and f_n, g_n, h_n are given by

$$\begin{aligned} f_n &= \cosh(\bar{n} - 1)s + \epsilon_B \sinh(\bar{n} - 1)s, \\ g_n &= 2\bar{n} \cosh s (\sinh \bar{n}s + \cosh \bar{n}s) + (\epsilon_B - 1) \sinh s \sinh \bar{n}s, \\ h_n &= \alpha(1 - \epsilon_B)e^{-\bar{n}s}(ne^s - (n + 1)e^{-s}). \end{aligned}$$

For the reader's convenience, we recall $s = \cosh^{-1}(d/R)$ and $\alpha = R \sinh s$.

Appendix D. Poladian's image method for two spheres (review).

Here, we present a review of Poladian's image method for two dielectric spheres. First, we explain the image method when only a single sphere is placed in the whole space. Then we discuss an image series solution for two spheres in a uniform incident field. Finally, we consider the generalized image method for the case of multipole sources.

D.1. A single sphere. Suppose that a single sphere of radius R is centered at $(0, 0, 0)$. Let ϵ_B be the permittivity of the sphere. We also assume the background permittivity is $\epsilon_0 = 1$. Let $\tau = (\epsilon_B - 1)/(\epsilon_B + 1)$. When we locate a point charge Q at $(0, 0, c)$ with $c > R$, then it can be shown that the reaction potential is identical to the potential generated by the following two image sources [43, 41, 42]: (1) a point charge $Q' = -\tau(R/c)Q$ at $(0, 0, R^2/c)$ and (2) a continuous line source along the line segment from $(0, 0, 0)$ to $(0, 0, R^2/c)$ with a density function Λ given by

$$\Lambda(t) = \frac{\tau Q}{R(\epsilon + 1)} \left(\frac{R^2}{ct} \right)^{\frac{1}{2}(\tau+1)}, \quad t \in (0, R^2/c).$$

Poladian observed that the continuous line source can be well approximated by a point charge $-Q'$ at the center of the sphere $(0, 0, 0)$ provided that $|\epsilon_B|$ is large. In fact, this approximation becomes exact when $|\epsilon_B| = \infty$.

Therefore, Poladian's imaging rule for a single sphere can be summarized as follows: if a sphere of radius R is centered at $(0, 0, 0)$ and a point charge Q is located at $(0, 0, c)$, then the following two image charges are produced: (i) a point charge $Q' = -\tau(R/c)Q$ at $(0, 0, R^2/c)$ (ii) a point charge $-Q'$ at the center of the sphere $(0, 0, 0)$ [43, 41, 42]. Let us call the latter image charge *the neutralizing charge*.

D.2. Two spheres in a uniform field. Let us now consider the two spheres B_+ and B_- . Suppose that we locate a point charge of the magnitude ± 1 at the point $(0, 0, \pm z_0)$ in the sphere B_{\pm} , respectively. Due to the interaction between two spheres, an infinite sequence of image charges is generated along z -axis by Poladian's imaging rule. But it is difficult to keep track of all the image charges at each step of the

recursive imaging process. Poladian found that it is much simpler to initially neglect the neutralizing charges and later introduce an additional image sources.

By ignoring the neutralizing charge in Poladian's imaging rule, we obtain an infinite sequence of the image charges as follows: for $m = 0, 1, 2, \dots$, m -th image charge $\pm u_m$ is located at the point $\pm \mathbf{z}_m = (0, 0, \pm z_m)$ in the sphere B_{\pm} , respectively, where z_m and u_m satisfy the following recursive relations:

$$d - z_{k+1} = \frac{R^2}{d + z_k}, \quad u_{k+1} = \tau \frac{R}{d + z_k} u_k.$$

These recursive relations can be solved explicitly. To state the solutions for u_k and z_k , we introduce a parameter t_0 which satisfies $z_0 = \alpha \coth(s + t_0)$. Note that if the initial position is equal to the center of each sphere (that is, $z_0 = d = R \cosh s$), then it holds that $t_0 = 0$. Using this representation for z_0 and the hyper-trigonometric identities, one can see that the solutions for z_k and u_k are given as follows:

$$z_k = \alpha \coth(ks + s + t_0), \quad u_k = \tau^k \frac{\sinh(s + t_0)}{\sinh(ks + s + t_0)}.$$

Then the potential $U(\mathbf{r})$ generated by all the above image charges is given by

$$(29) \quad U(\mathbf{r}) = \sum_{k=0}^{\infty} u_k (G(\mathbf{r} - \mathbf{z}_k) - G(\mathbf{r} + \mathbf{z}_k)),$$

where $\mathbf{z}_k = (0, 0, z_k)$.

Let us now consider the two spheres $B_+ \cup B_-$ placed in a uniform incident field $(0, 0, E_0)$. Let p_0 be the induced polarizability when a single sphere is subjected to the uniform incident field, that is, $p_0 = E_0 R^3 2\tau / (3 - \tau)$. We also let $D(\mathbf{r}) = \mathbf{e}_z \cdot \hat{\mathbf{r}} / (|\mathbf{r}|^2)$ be the potential generated by a point dipole source with a unit moment \mathbf{e}_z , where $\hat{\mathbf{r}} = \mathbf{r} / |\mathbf{r}|$. The uniform incident field is first imaged in each sphere, inducing an image point dipole source with the polarizability p_0 at the center of each sphere. Then these initial point dipoles produce an infinite sequence of image sources. The point dipole p_0 can be considered as the limit of two initial charges $\pm 4\pi p_0 / 2h$ at the points $z_0 = (0, 0, d \pm h)$ as $h \rightarrow 0$. It is equivalent to taking derivative $4\pi p_0 \partial / \partial z_0$ at $z_0 = d$. So we get the following expression for the image potential generated by the point dipole p_0 [43, 41, 42]:

$$(30) \quad V_1(\mathbf{r}) := 4\pi p_0 \frac{\partial(U(\mathbf{r}))}{\partial z_0} \Big|_{z_0=d}.$$

Then, from (29) and the identity $\frac{\partial}{\partial z_0} \Big|_{z_0=d} = -\frac{\sinh^2 s}{\alpha} \frac{\partial}{\partial t_0} \Big|_{t_0=0}$, we can represent V_1 more explicitly as follows:

$$V_1(\mathbf{r}) = \sum_{k=0}^{\infty} p_k D(\mathbf{r} - \mathbf{r}_k) - q_k G(\mathbf{r} - \mathbf{r}_k) + \sum_{k=0}^{\infty} p_k D(\mathbf{r} + \mathbf{r}_k) + q_k G(\mathbf{r} + \mathbf{r}_k),$$

where \mathbf{r}_k, p_k and q_k are given by

$$\mathbf{r}_k = \mathbf{z}_k|_{t_0=0} = (0, 0, \alpha \coth(k+1)s),$$

$$p_k = \tau^k p_0 \left(\frac{\sinh s}{\sinh(k+1)s} \right)^3, \quad q_k = \tau^k \frac{p_0}{R} \frac{\sinh s \sinh ks}{\sinh^2(k+1)s}.$$

Note that $\pm \mathbf{r}_0$ is the center of the sphere B_{\pm} , respectively.

As pointed out by Poladian in [43], the potential V_1 is unphysical because the total charge on each sphere is non-zero. It originates from the fact that we have ignored the neutralizing image charges. Now we explain Poladian's strategy for neutralizing the total charge [43]. We introduce an additional potential by locating a point charge $\pm Q$ at the center of the sphere B_{\pm} , respectively. Then the corresponding image potential is given by

$$V_2(\mathbf{r}) := QU(\mathbf{r})|_{z_0=d} = Q \sum_{k=0}^{\infty} u_k^0 (G(\mathbf{r} - \mathbf{r}_k) - G(\mathbf{r} + \mathbf{r}_k)),$$

where u_k^0 is defined by $u_k^0 = u_k|_{t_0=0} = \tau^k \sinh s / \sinh(k+1)s$. Now we choose the constant Q so that the potential $V_1 + V_2$ has no net flux on each sphere. More precisely, we impose $\int_{\partial B_{\pm}} \frac{\partial}{\partial \mathbf{n}} (V_1 + V_2) dS = 0$. Then we obtain $Q = \sum_{k=0}^{\infty} q_k / \sum_{k=0}^{\infty} u_k^0$. Finally, we get the approximation for the potential $V(\mathbf{r})$ by superposing the uniform incident field and the aforementioned potentials:

$$(31) \quad V(\mathbf{r}) + E_0 z \approx V_1(\mathbf{r}) + V_2(\mathbf{r}) = 4\pi p_0 \frac{\partial(U(\mathbf{r}))}{\partial z_0} \Big|_{z_0=d} + QU(\mathbf{r})|_{z_0=d}.$$

D.3. Image method for general multipole sources. We now consider the case when an initial image source is a multipole source \mathcal{Y}_{lm} . Note that, since the point charge potential G and the dipole potential D satisfy $G(\mathbf{r}) = \frac{1}{4\pi} \mathcal{Y}_{00}(\mathbf{r})$ and $D(\mathbf{r}) = \mathcal{Y}_{10}(\mathbf{r})$, the image potentials (7) and (30) can be seen as the special cases of potentials generated by the image multipole sources.

Before considering a general multipole source \mathcal{Y}_{lm} , let us first consider a sectoral multipole $\mathcal{Y}_{|m|,m}$. If an initial sectoral multipole $\mathcal{Y}_{|m|,m}$ is located at $(0, 0, z_0)$, the image sequence is produced by Poladian's rule [43, 41, 42] as follows: $u_m^{(2k)} \mathcal{Y}_{|m|,m}$ at $(0, 0, z_{2k})$ and $-u_m^{(2k+1)} \mathcal{Y}_{|m|,m}$ at $(0, 0, -z_{2k+1})$ for $k = 0, 1, 2, \dots$. Similarly, if an initial location is $(0, 0, -z_0)$, then the following image sequence is produced: $u_m^{(2k)} \mathcal{Y}_{|m|,m}$ at $(0, 0, -z_{2k})$ and $-u_m^{(2k+1)} \mathcal{Y}_{|m|,m}$ at $(0, 0, +z_{2k+1})$ for $k = 0, 1, 2, \dots$. Here, $u_m^{(k)}$ satisfies a recursive relation

$$u_m^{(k+1)} = \tau \left(\frac{R}{d + z_k} \right)^{2|m|+1} u_m^{(k)}, \quad k = 0, 1, 2, \dots$$

It can be explicitly solved as follows:

$$u_m^{(k)} = \tau^k \left(\frac{\sinh(s + t_0)}{\sinh(ks + s + t_0)} \right)^{2|m|+1}.$$

Let U_m^{\pm} be the potential generated by the above image sequence when the initial sectoral multipole is located at $(0, 0, \pm z_0)$, respectively. Then the potential U_m^{\pm} is given by

$$(32) \quad U_m^{\pm}(\mathbf{r}) = \sum_{k=0}^{\infty} u_m^{(2k)} \mathcal{Y}_{|m|,m}(\mathbf{r} \mp \mathbf{z}_{2k}) - u_m^{(2k+1)} \mathcal{Y}_{|m|,m}(\mathbf{r} \pm \mathbf{z}_{2k+1}).$$

Let us turn to the case of a general multipole source $\mathcal{Y}_{lm}(\mathbf{r})$. Let U_{lm}^{\pm} be the potential due to the image sequence produced by an initial multipole source \mathcal{Y}_{lm} located

at the center of the sphere B_{\pm} , respectively. It was shown that a general multipole source \mathcal{Y}_{lm} can be represented as a derivative of a sectoral multipole $\mathcal{Y}_{|m|,m}$ [43, 41, 42]:

$$(33) \quad \mathcal{Y}_{lm}(\mathbf{r} \mp \mathbf{r}_0) = \mathcal{D}_{lm}^{\pm} [\mathcal{Y}_{|m|,m}(\mathbf{r} \mp \mathbf{z}_0)],$$

where the differential operator \mathcal{D}_{lm}^{\pm} is defined by

$$(34) \quad \mathcal{D}_{lm}^{\pm}[f] = \frac{(\pm 1)^{l-|m|}}{N_{lm}} \frac{\partial^{l-|m|}}{\partial [z_0(t_0)]^{l-|m|}} f \Big|_{z_0=d},$$

where N_{lm} is defined as (21). Therefore, the image potential U_{lm}^{\pm} is also represented as $U_{lm}^{\pm}(\mathbf{r}) = \mathcal{D}_{lm}^{\pm}[U_m^{\pm}(\mathbf{r})]$. Actually, this is not the end. We need to be careful when we consider the case when $m = 0$. In this case, the total charges on each sphere B_{\pm} may be non-zero. Since this is unphysical, we have to neutralize them again. We modify the potential U_{lm}^+ by adding an image potential produced by the following initial charges: a point charge $-Q_{l,1}^+$ (and $-Q_{l,2}^+$) at the center of the sphere B_+ (and B_-), respectively. We also modify the potential U_{lm}^- in a similar way with the initial charges $-Q_{l,i}^-$, $i = 1, 2$. Here, the constants $Q_{l,i}^{\pm}$ are chosen so that the total flux on each surface ∂B_{\pm} is zero. Specifically, the potential $U_{l,m}^{\pm}$ is modified as follows:

$$(35) \quad U_{lm}^{\pm}(\mathbf{r}) = \mathcal{D}_{lm}^{\pm}[U_m^{\pm}(\mathbf{r})] - \delta_{0m} Q_{l,1}^{\pm} U_0^+(\mathbf{r})|_{z_0=d} - \delta_{0m} Q_{l,2}^{\pm} U_0^-(\mathbf{r})|_{z_0=d},$$

where δ_{lm} is the Kronecker delta.

It is worth to remark that we can evaluate the derivatives $\mathcal{D}_{lm}^{\pm}[f]$ analytically by using the Faà di Bruno's formula (we omit the details). Moreover, its numerical computation can be done efficiently using a recursive relation for Bell polynomials.

Appendix E. Proof of Lemma 6.1. From the definition (22) of the bispherical coordinates, we have $z + i\rho = 2\alpha/(e^{\xi-i\eta} - 1) + \alpha$. Note that $\coth t = 2/(e^{2t} - 1) + 1$. Hence, by using these identities and letting $\mathbf{z}(t) = (0, 0, \alpha \coth t)$, it follows that

$$(36) \quad \frac{1}{|\mathbf{r} - \mathbf{z}(t)|} = |z + i\rho - \alpha \coth t|^{-1} = \frac{1}{2\alpha} \left| \frac{1}{e^{\xi-i\eta} - 1} - \frac{1}{e^{2t} - 1} \right|^{-1} \\ = \frac{1}{2\alpha} \left| \frac{(e^{2t} - 1)(e^{\xi-i\eta} - 1)}{e^{2t}(e^{\xi-2t-i\eta} - 1)} \right| = \frac{\sinh |t|}{\alpha} \frac{\sqrt{\cosh \xi - \cos \eta}}{\sqrt{\cosh(\xi - 2t) - \cos \eta}}.$$

By letting $a = e^{-|\xi-2t|}$ and $x = \cos \eta$ in (16), it is easy to check that

$$\frac{1}{\sqrt{\cosh(\xi - 2t) - \cos \eta}} = \sqrt{2} \sum_{n=0}^{\infty} e^{-(n+\frac{1}{2})|\xi-2t|} P_n(\cos \eta).$$

Then, for $\xi < 2t$, we have

$$(37) \quad \frac{\alpha}{\sinh |t|} \frac{1}{|\mathbf{r} - \mathbf{z}(t)|} = \sqrt{2} \sqrt{\cosh \xi - \cos \eta} \sum_{n=0}^{\infty} e^{-(2n+1)t} e^{(n+\frac{1}{2})\xi} P_n(\cos \eta).$$

Using the fact that $z_0 = (0, 0, \alpha \coth(s + t_0)) \in B_+$, it can be shown that $t_0 > -s/2$. It implies that $\xi < 2(ks + s + t_0)$ for $|\xi| \leq s$. Recall that $|\xi| \leq s$ for $\mathbf{r} \in \mathbb{R}^3 \setminus (B_+ \cup B_-)$. Hence (37) holds for $t = ks + s + t_0$ and $\mathbf{r} \in \mathbb{R}^3 \setminus (B_+ \cup B_-)$. Note that $\mathbf{z}_k = \mathbf{z}(ks + s + t_0)$.

Therefore, using (26) and the definitions of u_k and G , the conclusion follows for $u_k G(\mathbf{r} - \mathbf{z}_k)$. The other case for $u_k G(\mathbf{r} + \mathbf{z}_k)$ can be considered in the same way.

Appendix F. Proof of Theorem 7.1. We shall prove the result by applying our connection formula to Poladian's image series solution. From the image solution (31), Theorem 6.2 and the identity $\partial_{z_0}|_{z_0=d} = -(\sinh^2 s/\alpha)\partial_{t_0}|_{t_0=0}$, we get

$$\begin{aligned}
 (38) \quad V(\mathbf{r}) + E_0 z &\approx V_1(\mathbf{r}) + V_2(\mathbf{r}) = 4\pi p_0 \partial_{z_0}|_{z_0=d} U(\mathbf{r}) + Q U(\mathbf{r})|_{z_0=d} \\
 &= E_0 \frac{2\tau\alpha}{3-\tau} \sum_{n=0}^{\infty} \frac{2n+1 - \coth s}{e^{(2n+1)s} - \tau} (\mathcal{M}_{n,+}^0(\mathbf{r}) - \mathcal{M}_{n,-}^0(\mathbf{r})) \\
 &\quad + Q \sum_{n=0}^{\infty} \frac{\mathcal{M}_{n,+}^0(\mathbf{r}) - \mathcal{M}_{n,-}^0(\mathbf{r})}{e^{(2n+1)s} - \tau}.
 \end{aligned}$$

Now let us consider the constant Q . Recall the following condition:

$$\int_{\partial B_+} \frac{\partial}{\partial \mathbf{n}} (V_1 + V_2) dS = 0.$$

Then, by using Theorem K.4, we obtain

$$E_0 \frac{2\tau\alpha}{3-\tau} \sum_{n=0}^{\infty} \frac{2n+1 - \coth s}{e^{(2n+1)s} - \tau} + Q \sum_{n=0}^{\infty} \frac{1}{e^{(2n+1)s} - \tau} = 0.$$

Hence, we see that $Q = -K_0 + E_0 \frac{2\tau\alpha}{3-\tau} \coth s$. Therefore, from (38), the conclusion follows.

Appendix G. Proof of Theorem 8.1. We first consider the case of a sectoral multipole $\mathcal{Y}_{|m|,m}$. We can represent the image potential $u_m^{(k)} \mathcal{Y}_{|m|,m}(\mathbf{r} \mp \mathbf{z}_k)$ using TO basis as follows.

LEMMA G.1. (*Converting image sectoral multipole to TO*) For $\mathbf{r} \in \mathbb{R}^3 \setminus (B_+ \cup B_-)$, we have

$$u_m^{(k)} \mathcal{Y}_{|m|,m}(\mathbf{r} \mp \mathbf{z}_k) = \sum_{n=|m|}^{\infty} g_n^m \lambda_n^m [\tau e^{-(2n+1)s}]^k e^{-(2n+1)s} \mathcal{M}_{n,\pm}^m(\mathbf{r}),$$

where λ_n^m and g_n^m are given in (15).

Proof. For simplicity, we consider only $u_m^{(k)} \mathcal{Y}_{|m|,m}(\mathbf{r} - \mathbf{z}_k)$. From (18) and the fact that $\rho = |\mathbf{r} - \mathbf{z}_k| \sin \theta_k$, we have

$$\begin{aligned}
 (39) \quad \mathcal{Y}_{|m|,m}(\mathbf{r} - \mathbf{z}_k) &= \frac{1}{\sqrt{(2|m|)!}} \frac{P_{|m|}^{(m)}(\cos \theta_k) e^{im\phi_k}}{|\mathbf{r} - \mathbf{z}_k|^{|m|+1}} \\
 &= \omega_m \frac{[\sin \theta_k]^{|m|} e^{im\phi_k}}{|\mathbf{r} - \mathbf{z}_k|^{|m|+1}} = \omega_m \frac{\rho^{|m|} e^{im\phi_k}}{|\mathbf{r} - \mathbf{z}_k|^{|2|m|+1}},
 \end{aligned}$$

where $\omega_m = (-1)^{|m|} (2|m| - 1)!! / \sqrt{(2|m|)!}$ and (r_k, θ_k, ϕ_k) is the spherical coordinates system for $\mathbf{r} - \mathbf{z}_k$. Note that $\phi_k = \varphi$ for all $k \geq 0$.

From (36) and the fact that $\mathbf{z}_k = \mathbf{z}(ks + s + t_0)$, we see that

$$\frac{1}{|\mathbf{r} - \mathbf{z}_k|} = \frac{\sin(ks + s + t_0)\sqrt{\cosh \xi - \cos \eta}}{\alpha\sqrt{\cosh(\xi - 2(ks + s + t_0)) - \cos \eta}}.$$

We also have from (23) that $\rho = \alpha \sin \eta / (\cosh \xi - \cos \eta)$. By substituting these expressions for $1/|\mathbf{r} - \mathbf{z}_k|$ and ρ into (39), we get

$$(40) \quad u_m^{(k)} \mathcal{Y}_{|m|,m}(\mathbf{r} - \mathbf{z}_k) = \tau^k \frac{\sinh^{2|m|+1}(s + t_0)}{\sqrt{(2|m|)!} \alpha^{|m|+1}} \sqrt{\cosh \xi - \cos \eta} \\ \times \frac{2^{|m|+1/2} (-1)^{|m|} (2|m| - 1)!! [\sin \eta]^{|m|} e^{im\phi_k}}{[2(\cosh(\xi - 2(ks + s + t_0)) - \cos \eta)]^{|m|+1/2}}.$$

By letting $a = e^{-|\xi-2t|}$ and $x = \cos \eta$ in (17), it is easy to check that

$$\frac{(-1)^m (2m - 1)!! [\sin \eta]^m}{[2(\cosh(\xi - 2t) - \cos \eta)]^{m+1/2}} = \sum_{n=m}^{\infty} e^{-(n+\frac{1}{2})|\xi-2t|} P_n^m(\cos \eta).$$

By applying this identity to (40) with $t = ks + s + t_0$, we obtain that

$$u_m^{(k)} \mathcal{Y}_{|m|,m}(\mathbf{r} - \mathbf{z}_k) = \tau^k 2^{|m|} \frac{\sinh^{2|m|+1}(s + t_0)}{\sqrt{(2|m|)!} \alpha^{|m|+1}} \sqrt{2} \sqrt{\cosh \xi - \cos \eta} \\ \times \sum_{n=|m|}^{\infty} e^{-(2n+1)(ks+s+t_0)} e^{(n+\frac{1}{2})\xi} P_n^{|m|}(\cos \eta) e^{im\varphi},$$

for $|\xi| \leq s$. Then, from (26), the conclusion follows. \square

Now we are ready to prove Theorem 8.1. By applying Lemma G.1 to (32) and then using the following identity:

$$(41) \quad \sum_{k=0}^{\infty} [\tau e^{-(2n+1)s}]^{2k} = \frac{e^{2(2n+1)s}}{e^{2(2n+1)s} - \tau^2},$$

we obtain

$$U_m^{\pm}(\mathbf{r}) = \sum_{n=|m|}^{\infty} g_n^m \lambda_n^m \frac{e^{(2n+1)s} \mathcal{M}_{n,\pm}^m(\mathbf{r}) - \tau \mathcal{M}_{n,\mp}^m(\mathbf{r})}{e^{2(2n+1)s} - \tau^2}.$$

Then, by using (35), we get

$$(42) \quad U_{lm}^{\pm}(\mathbf{r}) = \sum_{n=|m|}^{\infty} \frac{g_n^m \mathcal{D}_{lm}^{\pm}[\lambda_n^m]}{e^{2(2n+1)s} - \tau^2} (e^{(2n+1)s} \mathcal{M}_{n,\pm}^m(\mathbf{r}) - \tau \mathcal{M}_{n,\mp}^m(\mathbf{r})) \\ - \delta_{0m} Q_{l,1}^{\pm} \frac{\sinh s}{\alpha} \sum_{n=0}^{\infty} \frac{e^{(2n+1)s} \mathcal{M}_{n,+}^0(\mathbf{r}) - \tau \mathcal{M}_{n,-}^0(\mathbf{r})}{e^{2(2n+1)s} - \tau^2} \\ - \delta_{0m} Q_{l,2}^{\pm} \frac{\sinh s}{\alpha} \sum_{n=0}^{\infty} \frac{(-\tau) \mathcal{M}_{n,+}^0(\mathbf{r}) + e^{(2n+1)s} \mathcal{M}_{n,-}^0(\mathbf{r})}{e^{2(2n+1)s} - \tau^2}.$$

Now we consider the following flux conditions:

$$\int_{\partial B_+} \frac{\partial(U_{l,m}^\pm)}{\partial \mathbf{n}} dS = 0, \quad \int_{\partial B_-} \frac{\partial(U_{l,m}^\pm)}{\partial \mathbf{n}} dS = 0.$$

Then, by applying Theorem K.4 to the above conditions with (42), we obtain

$$Q_{l,1}^\pm \frac{\sinh s}{\alpha} = \frac{\tilde{Q}_{l,1}^\pm \pm \tilde{Q}_{l,2}^\pm}{2}, \quad Q_{l,2}^\pm \frac{\sinh s}{\alpha} = (-1)^l \frac{\tilde{Q}_{l,1}^\pm \mp \tilde{Q}_{l,2}^\pm}{2}.$$

By rearranging the terms, the proof is completed.

Appendix H. Field at the gap center and absorption cross section.

From (28), we can see that the magnitude of the electric field at the gap is given by

$$E = -(\nabla V \cdot \mathbf{e}_z)(0, 0, 0) = E_0 - \frac{2^{3/2}}{\alpha} \sum_{n=0}^{\infty} A_n (2n+1) (-1)^n.$$

As mentioned in the main text, the absorption cross section σ_a is given by $\sigma_a = \omega \text{Im}\{p\}$ where p is the polarizability. It was shown in [17] that the polarizability p is given by $p = \sqrt{2}\alpha^2 \sum_{n=0}^{\infty} (2n+1) A_n$. Therefore, by replacing A_n by \tilde{A}_n , we can derive approximate analytical expressions for E and σ_a .

Appendix I. Multipole expansion method. The classical way to solve the many-spheres problem is Rayleigh's multipole expansion method. Here, we briefly review this method. Recall that the solid harmonics \mathcal{Y}_{lm} and \mathcal{Z}_{lm} are defined by

$$\mathcal{Y}_{lm}(\mathbf{r}) = \frac{Y_l^m(\theta, \phi)}{r^{l+1}}, \quad \mathcal{Z}_{lm}(\mathbf{r}) = r^l Y_l^m(\theta, \phi).$$

Any solution to Laplace's equation can be represented as a sum of \mathcal{Y}_{lm} and \mathcal{Z}_{lm} . The solution $V(\mathbf{r})$ to the problem (2) can be represented as the following multipole expansion: for \mathbf{r} belonging to the region outside the spheres, we have

$$(43) \quad V(\mathbf{r}) = -E_0 z + \sum_{j=1}^J \sum_{l=1}^{\infty} \sum_{m=-l}^l C_{j,lm} \mathcal{Y}_{lm}(\mathbf{r} - \mathbf{c}_j),$$

where the coefficients $C_{j,lm}$ are unknown constants and \mathbf{c}_j is the center of the sphere B_j . For the inner region of B_j , we can easily extend the above representation by imposing the continuity of the potential on the surface ∂B_j . For $\mathbf{r} \in B_j$, we have

$$V(\mathbf{r}) = \sum_{l=0}^{\infty} \sum_{m=-l}^l C_{j,lm} \frac{\mathcal{Z}_{lm}(\mathbf{r} - \mathbf{c}_j)}{R^{2l+1}}.$$

Then, by using the addition formula (46) for \mathcal{Y}_{lm} and the transmission condition, $\nabla V \cdot \mathbf{n}|_+ = \epsilon_B \nabla V \cdot \mathbf{n}|_-$ on the surface ∂B_j , the infinite dimensional linear system for unknowns $C_{j,lm}$ can be derived. If all the spheres are well-separated, good accuracy can be achieved by truncating the linear system by a small order. But, if some of the spheres are close to touching, the charge densities on their surfaces become nearly singular. So more harmonics are required to describe them accurately.

Appendix J. Hybrid numerical scheme for many plasmonic spheres.

Here we present our hybrid numerical scheme for computing the field generated

by plasmonic spheres clusters. We modify Cheng and Greengard's hybrid method [12, 10, 15] by using our connection formulas between TO and the image method. So we first explain their idea in detail and then explain how we modify it for the plasmonic spheres system.

J.1. Cheng and Greengard's hybrid method. To illustrate the idea of the hybrid numerical schemes in [12, 10, 15], let us consider an example of three spheres (that is, $N = 3$). Suppose that the spheres B_1 and B_2 are closely located but well-separated from B_3 . Then the charge density on ∂B_3 can be well represented by a low-order spherical harmonics expansion. But the charge densities both on ∂B_1 and ∂B_2 may be singular, so it is better to use the image method to describe their associated potentials. In view of this observation, they modified the multipole expansion as follows: for \mathbf{r} belonging to the region outside the spheres,

$$V(\mathbf{r}) = -E_0 z + \sum_{j=1}^2 \sum_{l=1}^{\infty} \sum_{m=-l}^l C_{12,lm} U_{12,lm}(\mathbf{r}) + \sum_{l=1}^{\infty} \sum_{m=-l}^l C_{3,lm} \mathcal{Y}_{lm}(\mathbf{r} - \mathbf{c}_3),$$

where $U_{12,lm}$ is the image series solution which includes all the image sources induced from the multipoles $C_{j,lm} \mathcal{Y}_{lm}(\mathbf{r} - \mathbf{c}_j)$, $j = 1, 2$, by the interaction between two spheres B_1 and B_2 . This representation for $V(\mathbf{r})$ can be directly generalized to a system of an arbitrary number of spheres. The resulting scheme is extremely efficient and accurate even if the spheres are nearly touching. This is because the close-to-touching interaction is already captured in the image multipole series.

J.2. Outline of the modified algorithm for plasmonic spheres. As already mentioned, the image-series-based hybrid method cannot be applied for plasmonic spheres due to the non-convergence of the image series. Our strategy for extending the hybrid method to the case of plasmonic spheres is to convert the image multipole series to their TO-type versions using the connection formula for general multipoles (Theorem 8.1). As a result, we obtain the modified hybrid numerical scheme valid for plasmonic spheres clusters. Here, we present the outline of the algorithm of our proposed scheme.

1. Write down the potential $V(\mathbf{r})$ in the multipole expansion form as in (43).
2. If a pair of spheres, say B_j and B_k , are closely located (if the separation distance is smaller than a given number, for example, the radius R), then we rotate the xyz -axis for both $\mathbf{r} - \mathbf{c}_j$ and $\mathbf{r} - \mathbf{c}_k$ so that the $+z$ -axis is in the direction of the axis of the pair of spheres, that is, $\mathbf{c}_j - \mathbf{c}_k$.
3. We also transform the multipole expansion for B_j into the rotated frame using (47). Let us denote the coefficients in the rotated frame by $C'_{j,lm}$.
4. By using the connection formula for general multipoles (Theorem 8.1), we modify the multipole expansion in the rotated frame by replacing $C'_{j,lm} \mathcal{Y}_{lm}(\mathbf{r})$ with the hybrid TO multipole $C'_{j,lm} U_{lm}^+(\mathbf{r})$.
5. Do the same as in step 4 for B_k with $U_{lm}^-(\mathbf{r})$ instead of $U_{lm}^+(\mathbf{r})$.
6. We convert the TO-type expansion for B_j and B_k into the form of multipole expansion using Theorem K.3.
7. Rotate the axis of the coordinate system and transform the multipole expansions into the original frame.
8. Perform steps 2-7 for all the pairs of closely spaced spheres.
9. We extend the resulting multipole expansion to the inner regions of B_j for $j = 1, 2, \dots, N$ using Theorem K.2.

10. By applying the addition formula (46) for \mathcal{Y}_{lm} with the transmission conditions on ∂B_j , we construct the infinite dimensional linear system for unknowns $C_{j,lm}$.
11. We solve the linear system after a truncation.

Appendix K. Useful formulas. Here we collect many useful formulas.

K.1. Potential inside two spheres. The following theorems are useful for finding a potential inside the two spheres when we have an explicit representation of the potential in the outside region.

THEOREM K.1. *Suppose that V satisfies the Laplace equation inside and outside the two spheres B_+ and B_- . We also assume that the potential V is continuous on each surface ∂B_{\pm} . We also assume that, outside the spheres, the potential V is given by*

$$V(\mathbf{r}) = \sum_{n=0}^{\infty} \sum_{m=-n}^n a_{n,+}^m \mathcal{M}_{n,+}^m(\mathbf{r}) + a_{n,-}^m \mathcal{M}_{n,-}^m(\mathbf{r}),$$

for $\mathbf{r} \in \mathbb{R}^3 \setminus (B_+ \cup B_-)$ and some coefficients $a_{n,\pm}^m$. Then, inside the spheres, the potential $V(\mathbf{r})$ for $\mathbf{r} \in B_{\pm}$ is given by

$$V(\mathbf{r}) = \sum_{n=0}^{\infty} \sum_{m=-n}^n (a_{n,\pm}^m e^{(2n+1)s} + a_{n,\mp}^m) \mathcal{M}_{n,\mp}^m(\mathbf{r}),$$

Proof. It is obvious that the series on the right-hand side satisfies the Laplace equation. Since $\partial B_{\pm} = \{\xi = \pm s\}$, we have the following identity:

$$\begin{aligned} \mathcal{M}_{n,+}^m(\mathbf{r})|_{\partial B_{\pm}} &= \sqrt{2} \sqrt{\cosh \xi - \cos \eta} e^{\pm(n+1/2)s} Y_n^m(\eta, \varphi) \\ &= e^{\pm(2n+1)s} \mathcal{M}_{n,-}^m(\mathbf{r})|_{\partial B_{\pm}}. \end{aligned}$$

Then one can easily check that the potential V is continuous on each surface $\partial B_{\pm} = \{\xi = \pm s\}$. The proof is completed. \square

THEOREM K.2. *Suppose that V satisfies the Laplace equation inside and outside the two spheres B_+ and B_- . We also assume that the potential V is continuous on each surface ∂B_{\pm} . Furthermore, we assume that, outside the spheres, the potential V is given by*

$$V(\mathbf{r}) = \sum_{l=0}^{\infty} \sum_{m=-l}^l f_{lm}^+ \mathcal{Y}_{lm}(\mathbf{r} - \mathbf{r}_0) + f_{lm}^- \mathcal{Y}_{lm}(\mathbf{r} + \mathbf{r}_0),$$

for $\mathbf{r} \in \mathbb{R}^3 \setminus (B_+ \cup B_-)$ and some coefficients $f_{l,m}^{\pm}$. Then, inside the spheres, the potential $V(\mathbf{r})$ for $\mathbf{r} \in B_{\pm}$ is given by

$$V(\mathbf{r}) = \sum_{l=0}^{\infty} \sum_{m=-l}^l \frac{f_{lm}^+}{R^{2l+1}} \mathcal{Z}_{lm}(\mathbf{r} - \mathbf{r}_0) + \frac{f_{lm}^-}{R^{2l+1}} \mathcal{Z}_{lm}(\mathbf{r} + \mathbf{r}_0).$$

Proof. The conclusion immediately follows from the definition of the solid harmonics \mathcal{Y}_{lm} and \mathcal{Z}_{lm} . \square

K.2. From TO to multipole expansion. When we apply our hybrid numerical scheme for plasmonic spheres, we need to convert a TO-type solution into a multipole expansion. Let us consider the following general potential W_{\pm} in the form of TO solution:

$$(44) \quad W_{\pm}(\mathbf{r}) = \sum_{n=0}^{\infty} \sum_{m=-n}^n a_{n,\pm}^m \mathcal{M}_{n,\pm}^m(\mathbf{r}),$$

for some coefficients $a_{n,\pm}^m$. We want to convert the potential W_{\pm} into a multipole expansion form as follows:

$$(45) \quad W_{\pm}(\mathbf{r}) = \begin{cases} \sum_{l=0}^{\infty} \sum_{m=-n}^n c_{lm}^{\pm} \mathcal{Y}_{lm}(\mathbf{r} \mp \mathbf{r}_0), & \mathbf{r} \in \mathbb{R}^3 \setminus B_{\pm}, \\ \sum_{l=0}^{\infty} \sum_{m=-n}^n d_{lm}^{\pm} \mathcal{Z}_{lm}(\mathbf{r} \mp \mathbf{r}_0), & \mathbf{r} \in B_{\pm}, \end{cases}$$

where the coefficients c_{lm}^{\pm} and d_{lm}^{\pm} are to be determined. We derive explicit formulas for c_{lm}^{\pm} and d_{lm}^{\pm} in the following theorem. Its proof is given in Appendix L.

THEOREM K.3. (*Conversion of TO solution into multipole expansion*) *The multipole coefficients c_{lm}^{\pm} and d_{lm}^{\pm} are represented in terms of TO coefficients $a_{n,\pm}^m$ as follows:*

$$\begin{cases} c_{lm}^{\pm} = 2\alpha R^{2l+1} \sum_{n=|m|}^{\infty} a_{n,\pm}^m g_n^m \mathcal{D}_{lm}^{\pm}[\lambda_n^m], \\ d_{lm}^{\pm} = 2\alpha \sum_{n=|m|}^{\infty} a_{n,\mp}^m e^{-(2n+1)s} g_n^m \mathcal{D}_{lm}^{\pm}[\lambda_n^m]. \end{cases}$$

In view of (45), the total flux on the surface ∂B_{\pm} is given as

$$\int_{\partial B_{\pm}} \frac{\partial W_{\pm}}{\partial \mathbf{n}} dS = 4\pi c_{00}^{\pm}, \quad \int_{\partial B_{\pm}} \frac{\partial W_{\mp}}{\partial \mathbf{n}} dS = 0.$$

So, we have the following flux formula from the above theorem.

THEOREM K.4. (*Total flux formula*) *Let W_{\pm} be the potential given as (44). Then the total flux on the surface ∂B_{\pm} is*

$$\int_{\partial B_{\pm}} \frac{\partial W_{\pm}}{\partial \mathbf{n}} dS = 8\pi\alpha \sum_{n=0}^{\infty} a_{n,\pm}^0, \quad \int_{\partial B_{\pm}} \frac{\partial W_{\mp}}{\partial \mathbf{n}} dS = 0.$$

K.3. Translation and rotation of multipole expansions. To apply the multipole expansion method, we need to represent a multipole source in a translated or rotated coordinate. It was shown that the following identities hold [43].

Translation: A translated multipole source $\mathcal{Y}_{lm}(\mathbf{r} - \mathbf{r}')$ can be expanded as

$$(46) \quad \mathcal{Y}_{lm}(\mathbf{r} - \mathbf{r}') = \sum_{a=0}^{\infty} \sum_{b=-a}^a w_m w_b w_{m-b} N_{lmab} (-1)^{l+a} \mathcal{Z}_{ab}(\mathbf{r}_{<}) \mathcal{Y}_{l+a,m-b}(\mathbf{r}_{>}),$$

where $\mathbf{r}_{<}$ is the smaller (in magnitude) of \mathbf{r} and \mathbf{r}' and $\mathbf{r}_{>}$ is the larger. Here w_m and N_{lmab} are defined as (19) and (20), respectively.

Rotation: Suppose that the coordinate axes are rotated through Euler angle α, β, γ . The point (θ, ϕ) becomes $(\tilde{\theta}, \tilde{\phi})$. The following result holds:

$$(47) \quad Y_{lm}(\theta, \phi) = \sum_{M=-l}^l w_m w_M D_{mM}^{(l)}(\alpha, \beta, \gamma) Y_l^M(\tilde{\theta}, \tilde{\phi}),$$

where $D_{mM}^{(l)}(\alpha, \beta, \gamma) = e^{-i\alpha + M\gamma} d_{mM}^l(\beta)$ and

$$\begin{aligned} d_{mM}^l(\beta) &= \cos(\beta/2)^{2l+m-M} \sin(\beta/2)^{M-m} \\ &\times \sum_t \sqrt{\binom{l+m}{t} \binom{l-M}{t} \binom{l+M}{l+m-t} \binom{l-m}{l-M-t}} \\ &\times (-1)^t \tan(\beta/2)^{2t}. \end{aligned}$$

The summation in t is carried over $\max(0, m-M) \leq t \leq \min(l+m, l-M)$.

Appendix L. Proof of Theorem K.3. Let σ_{\pm} be the charge density on the surface ∂B_{\pm} , respectively. Now let us decompose σ_{\pm} using the spherical harmonics $Y_l^m(\theta_{\pm}, \phi_{\pm})$, where $(r_{\pm}, \theta_{\pm}, \phi_{\pm})$ are the spherical coordinates for $\mathbf{r} \mp \mathbf{r}_0$, respectively. Let us write σ_{\pm} as

$$\sigma_{\pm} = \sum_{l=0}^{\infty} \sum_{m=-l}^l \sigma_{lm}^{\pm} Y_l^m(\theta_{\pm}, \phi_{\pm}).$$

Here, σ_{lm}^{\pm} can be determined using the orthogonality of the spherical harmonics as follows:

$$(48) \quad \sigma_{lm}^{\pm} = \frac{2l+1}{4\pi} \frac{1}{R^2} \int_{\partial B_{\pm}} \sigma_{\pm} \overline{Y_l^m}(\theta_{\pm}, \phi_{\pm}) dS.$$

To calculate the right-hand side of (48), we need to express σ_{\pm} and $Y_l^m(\theta_{\pm}, \phi_{\pm})$ in terms of TO harmonics $Y_n^m(\eta, \varphi)$.

First, let us consider σ_{\pm} . Let 'ext'(or 'int') denote the limit from the outside (or inside) the sphere, respectively. It is well-known that the electric field $\mathbf{E} = -\nabla W$ satisfies the following boundary condition on ∂B_{\pm} :

$$\mathbf{E} \cdot \mathbf{n}|_{ext} - \mathbf{E} \cdot \mathbf{n}|_{int} = \sigma_{\pm}, \quad \text{on } \partial B_{\pm}.$$

To use the above condition, we need an explicit expression for W_{\pm} in the region inside the spheres B_{\pm} , respectively. From Theorem K.1, we have, for $\mathbf{r} \in B_{\pm}$,

$$(49) \quad W_{\pm}(\mathbf{r}) = \sum_{n=0}^{\infty} \sum_{m=-n}^n a_{n,\pm}^m e^{(2n+1)s} \mathcal{M}_{n,\mp}^m(\mathbf{r}),$$

respectively. So, by using (27), we obtain

$$(50) \quad \begin{aligned} \sigma_{\pm} &= -\frac{\partial W}{\partial \mathbf{n}} \Big|_{\partial B_{\pm}}^{ext} + \frac{\partial W}{\partial \mathbf{n}} \Big|_{\partial B_{\pm}}^{int} \\ &= (2\alpha)^{1/2} [J(\eta)]^{-3/2} \sum_{n,m} a_{n,\pm}^m (2n+1) e^{(n+\frac{1}{2})s} Y_n^m(\eta, \varphi), \end{aligned}$$

where $J(\eta)$ is defined by $J(\eta) = \alpha/(\cosh s - \cos \eta)$.

Next, let us consider $Y_l^m(\theta_\pm, \phi_\pm)$. From (33) and Lemma G.1, we have for $\mathbf{r} \in \partial B_+$,

$$(51) \quad \begin{aligned} Y_l^m(\theta_\pm, \phi_\pm) &= R^{l+1} \mathcal{Y}_{lm}(\mathbf{r} \mp \mathbf{r}_0) = R^{l+1} \mathcal{D}_{lm}^\pm[\mathcal{Y}_{|m|,m}(\mathbf{r} \mp \mathbf{z}_0)] \\ &= R^{l+1} (2\alpha)^{1/2} [J(\eta)]^{-1/2} \sum_{n=|m|}^{\infty} g_n^m \mathcal{D}_{lm}^\pm[\lambda_n^m] e^{-(n+1/2)s} Y_n^m(\eta, \varphi). \end{aligned}$$

We are ready to compute σ_{lm}^+ . By substituting (50) and (51) into (48), we obtain

$$(52) \quad \begin{aligned} \sigma_{lm}^\pm &= \frac{2l+1}{4\pi} \frac{1}{R^2} \int_0^{2\pi} \int_0^\pi \sigma_\pm \overline{Y_{lm}}[J(\eta)]^2 \sin \eta \, d\eta \, d\varphi \\ &= (2l+1) 2\alpha R^{l-1} \sum_{n=|m|}^{\infty} a_{n,\pm}^m g_n^m \mathcal{D}_{lm}^\pm[\lambda_n^m]. \end{aligned}$$

It is easy to check that the potential generated by the charge densities $\sigma_\pm = \sum \sigma_{lm}^\pm Y_l^m$ is given as follows: for $\mathbf{r} \in \mathbb{R}^3 \setminus (B_+ \cup B_-)$,

$$W_\pm(\mathbf{r}) = \sum_{l,m} \sigma_{lm}^\pm \frac{R^{l+2}}{2l+1} \mathcal{Y}_{lm}(\mathbf{r} \mp \mathbf{r}_0).$$

By comparing the above expression and (45), we immediately arrive at

$$c_{lm}^\pm = \sigma_{lm}^\pm \frac{R^{l+2}}{2l+1}.$$

Then, the formula for c_{lm}^\pm follows from (52). For the case of d_{lm}^\pm , it can be proved in a similar way.

Acknowledgments. The authors would like to thank Ross C. McPhedran and Graeme W. Milton for pointing out the existence of Poladian's thesis [43].

REFERENCES

- [1] H. Ammari, G. Ciraolo, H. Kang, H. Lee, and K. Yun, Spectral analysis of the Neumann-Poincaré operator and characterization of the stress concentration in anti-plane elasticity, *Arch. Rational Mech. Anal.*, 208 (2013), pp. 275-304.
- [2] H. Ammari, Y. Deng, and P. Millien, Surface plasmon resonance of nanoparticles and applications in imaging, *Arch. Rational Mech. Anal.*, 220 (2016), pp. 109-153.
- [3] H. Ammari, H. Kang, H. Lee, J. Lee, and M. Lim, Optimal estimates for the electric field in two dimensions, *J. Math. Pures Appl.*, 88 (2007), pp. 307-324.
- [4] H. Ammari, P. Millien, M. Ruiz, and H. Zhang, Mathematical analysis of plasmonic nanoparticles: The scalar case, *Arch. Rational Mech. Anal.*, 224 (2017), pp. 597-658.
- [5] H. Ammari, M. Ruiz, S. Yu, and H. Zhang, Mathematical analysis of plasmonic resonances for nanoparticles: The full Maxwell equations, *J. Differential Equations*, 261 (2016), pp. 3615-3669.
- [6] K. Ando and H. Kang, Analysis of plasmon resonance on smooth domains using spectral properties of the Neumann-Poincaré operator, *J. Math. Anal. Appl.*, 435 (2016), pp. 162-178.
- [7] E. S. Bao, Y. Y. Li, and B. Yin, Gradient estimates for the perfect conductivity problem, *Arch. Rational Mech. Anal.*, 193 (2009), pp. 195-226.
- [8] J. Bao, H. Li, and Y. Li, Gradient estimates for solutions of the Lamé system with partially infinite coefficients, *Arch. Rational Mech. Anal.*, 215 (2015), pp. 307-351.
- [9] E. Bonnetier and F. Triki, On the spectrum of the Poincaré variational problem for two close-to-touching inclusions in 2d, *Arch. Rational Mech. Anal.*, 209 (2013), pp. 541-567.

- [10] H. Cheng, On the method of images for systems of closely spaced conducting spheres, *SIAM J. Appl. Math.*, 61 (2001), pp. 1324-1337.
- [11] H. Cheng and L. Greengard, On the numerical evaluation of electrostatic fields in dense random dispersions of cylinders, *J. Comput. Phys.*, 136 (1997), pp. 629-639.
- [12] H. Cheng and L. Greengard, A method of images for the evaluation of electrostatic fields in systems of closely spaced conducting cylinders, *SIAM J. Appl. Math.*, 58 (1998), pp. 122-141.
- [13] L. S. Dolin, To the possibility of comparison of three-dimensional electromagnetic systems with nonuniform anisotropic filling, *Izvestiya Vysshikh Uchebnykh Zavedenii. Radiofizika.*, 4 (1961), pp. 964-967.
- [14] R. Esteban, A. G. Borisov, P. Nordlander, and J. Aizpurua, Bridging quantum and classical plasmonics with a quantum-corrected model, *Nature Communications*, 3 (2012), pp. 825 EP-.
- [15] Z. Gan, S. Jiang, E. Luijten, and Z. Xu, A hybrid method for systems of closely spaced dielectric spheres and ions, *SIAM J. Sci. Comput.*, 38 (2016), pp. B375-B395.
- [16] Y. Gorb, Singular behavior of electric field of high-contrast concentrated composites, *Multiscale Model Simul.*, 13 (2015), pp. 1312-1326.
- [17] A. Goyette and A. Navon, Two dielectric spheres in an electric field, *Phys. Rev. B*, 13 (1976), pp. 4320-4327.
- [18] D. K. Gramotnev and S. I. Bozhevolnyi, Plasmonics beyond the diffraction limit, *Nature Photonics*, 4 (2010), pp. 83-91.
- [19] L. Greengard and V. Rokhlin, A fast algorithm for particle simulations, *J. Comput. Phys.*, 73 (1987), pp. 325-348.
- [20] A. Greenleaf, Y. Kurylev, M. Lassas, and G. Uhlmann, Cloaking devices, electromagnetic wormholes, and transformation optics, *SIAM Rev.*, 51 (2009), pp. 3-33.
- [21] H. Kang, H. Lee, and K. Yun, Optimal estimates and asymptotics for the stress concentration between closely located stiff inclusions, *Math. Ann.*, 363 (2015), pp. 1281-1306.
- [22] H. Kang, M. Lim, and K. Yun, Characterization of the electric field concentration between two adjacent spherical perfect conductors, *SIAM J. Appl. Math.*, 74 (2014), pp. 125-146.
- [23] J. B. Lassiter, H. Sobhani, J. A. Fan, J. Kundu, F. Capasso, P. Nordlander, and N. J. Halas, Fano resonances in plasmonic nanoclusters: Geometrical and chemical tunability, *Nano Letters*, 10 (2010), pp. 3184-3189.
- [24] J. Lekner, Near approach of two conducting spheres: Enhancement of external electric field, *J. Electrostatics*, 69 (2011), pp. 559-563.
- [25] J. Lekner, Electrostatics of two charged conducting spheres, *Proc. R. Soc. A*, 468 (2012), pp. 2829-2848.
- [26] M. Lim and S. Yu, Asymptotics of the solution to the conductivity equation in the presence of adjacent circular inclusions with finite conductivities, *J. Math. Anal. Appl.*, 421 (2015), pp. 131-156.
- [27] M. Lim and K. Yun, Blow-up of electric fields between closely spaced spherical perfect conductors, *Comm. Partial Differential Equations*, 34 (2009), pp. 1287-1315.
- [28] I. V. Lindell, Electrostatic image theory for the dielectric sphere, *Radio Science*, 27 (1992), pp. 1-8.
- [29] I. V. Lindell, J. C.-E. Sten, and K. I. Nikoskinen, Electrostatic image method for the interaction of two dielectric spheres, *Radio Science*, 28 (1993), pp. 319-329.
- [30] B. Lukyanchuk, N. I. Zheludev, S. A. Maier, N. J. Halas, P. Nordlander, H. Giessen, and C. T. Chong, The fano resonance in plasmonic nanostructures and metamaterials, *Nature Materials*, 9 (2010), pp. 707-715.
- [31] Y. Luo, R. Zhao, and J. B. Pendry, van der waals interactions at the nanoscale: The effects of nonlocality, *Proc. Nat. Acad. Sci. U.S.A.*, 111 (2014), pp. 18422-18427.
- [32] R. C. McPhedran and G. W. Milton, Transport properties of touching cylinder pairs and of the square array of touching cylinders, *Proc. R. Soc. A*, 411 (1987), pp. 313-326.
- [33] R. C. McPhedran, L. Poladian, and G. W. Milton, Asymptotic studies of closely spaced, highly conducting cylinders, *Proc. R. Soc. A*, 415 (1988), pp. 185-196.
- [34] C. Neumann, *Hydrodynamische Untersuchungen nebst einem Anhang uber die Probleme der Electrostatik und der magnetischen Induktion*, Teubner, Leipzig, 1883.
- [35] P. Nordlander, C. Oubre, E. Prodan, K. Li, and M. I. Stockman, Plasmon hybridization in nanoparticle dimers, *Nano Letters*, 4 (2004), pp. 899-903.
- [36] E. D. Palik, *Handbook of Optical Constants of Solids*, Academic, 1985.
- [37] J. B. Pendry, A. Aubry, D. R. Smith, and S. A. Maier, Transformation optics and subwavelength control of light, *Science*, 337 (2012), pp. 549-552.
- [38] J. B. Pendry, A. I. Fernandez-Dominguez, Y. Luo, and R. Zhao, Capturing photons with

- transformation optics, *Nature Physics*, 9 (2013), pp. 518-522.
- [39] J. B. Pendry, Y. Luo, and R. Zhao, Transforming the optical landscape, *Science*, 348 (2015), pp. 521-524.
 - [40] J. B. Pendry, D. Schurig, and D. R. Smith, Controlling electromagnetic fields, *Science*, 312 (2006), pp. 1780-1782.
 - [41] L. Poladian, General theory of electrical images in sphere pairs, *Quart. J. Mech. Appl. Math.*, 41 (1988), pp. 395-417.
 - [42] L. Poladian, Asymptotic behaviour of the effective dielectric constants of composite materials, *Proc. R. Soc. A*, 426 (1989), pp. 343-359.
 - [43] L. Poladian, *Effective Transport and Optical Properties of Composite Materials*. Ph.D. thesis, University of Sydney, 1990.
 - [44] E. Prodan, C. Radloff, N. J. Halas, and P. Nordlander, A hybridization model for the plasmon response of complex nanostructures, *Science*, 302 (2003), pp. 419-422.
 - [45] I. Romero, J. Aizpurua, G. W. Bryant, and F. J. G. de Abajo, Plasmons in nearly touching metallic nanoparticles: singular response in the limit of touching dimers, *Opt. Express*, 14 (2006), pp. 9988-9999.
 - [46] O. Schnitzer, Singular perturbations approach to localized surface-plasmon resonance: Nearly touching metal nanospheres, *Phys. Rev. B*, 92 (2015), p. 235428.
 - [47] O. Schnitzer, V. Giannini, R. V. Craster, and S. A. Maier, Asymptotics of surface-plasmon redshift saturation at subnanometric separations, *Phys. Rev. B*, 93 (2016), p. 041409.
 - [48] J. A. Schuller, E. S. Barnard, W. Cai, Y. C. Jun, J. S. White, and M. L. Brongersma, Plasmonics for extreme light concentration and manipulation, *Nature Materials*, 9 (2010), pp. 193-204.
 - [49] M. I. Stockman, Nanofocusing of optical energy in tapered plasmonic waveguides, *Phys. Rev. Lett.*, 93 (2004), p. 137404.
 - [50] L. A. Sweatlock, S. A. Maier, H. A. Atwater, J. J. Penninkhof, and A. Polman, Highly confined electromagnetic fields in arrays of strongly coupled ag nanoparticles, *Phys. Rev. B*, 71 (2005), p. 235408.
 - [51] K. Yun, Estimates for electric fields blown up between closely adjacent conductors with arbitrary shape, *SIAM J. Appl. Math.*, 67 (2007), pp. 714-730.
 - [52] K. Yun, An optimal estimate for electric fields on the shortest line segment between two spherical insulators in three dimensions, *J. Differential Equations*, 261 (2016), pp. 148-188.
 - [53] R. Zhao, Y. Luo, A. I. Fernandez-Domínguez, and J. B. Pendry, Description of van der Waals interactions using transformation optics, *Phys. Rev. Lett.*, 111 (2013), p. 033602.